Dear Editor,

First, we thank you for handing this manuscript. We revised the paper according to reviewer's comments and suggestions. The key revisions are summarized below and the paper is significantly improved. We hope that the revised paper could satisfy you and the referees, and that you now find it suitable for publication in ACP.

Best regards,

Tao

Summary of key revisions

The key revisions of the manuscript according to the reviewers' comments are summarized below by sections:

Title

The title was changed to 'Marine Boundary Layer Structure as Observed by A-Train Satellites' according to referee 1's specific comment (1).

1 2 Data

2 2.1 Satellite Observations and Data Collocation

(1) Information of CloudSat and AMSR-E was added according to referee 1's specific comment (7).

(2) According to referee 1's specific comment (12) and referee 2's comment (3), more information related to the evaluation of AMSR-E U10m and SST is provided now.

(3) Details of the data collocation were rephrased according to referee 1's major comment (1).

3 3 MBL Structure Identification Methodology

4 3.2 MBL structure identification methodology for CALIOP

(1) According to referee 2's major comment (2), additional evaluation results for the lidar-based MBL structure determination methodology with collocated clear-sky lidar and radiosonde measurements at the ARM Nauru site were added. The results show good accuracies of our lidar based BLH and MLH determinations for clear-sky MBL.

(2) Correlation coefficients and a measure of the statistical significance level were added for related results according to referee 1's major comment (3) and specific comment (20,30), referee 2's minor comment (6) and main issue (1), and referee 3's comment (1).

5 4 Results and Discussions

6 4.1 MBL Structure over the Eastern Pacific Ocean

(1) According to referee 3's comment (1), spatial correlations in Fig. 3, correlations between wind and EIS in Fig. 4 and 5, and uncertainties of MLH/BLH and EIS were quantified.

(2) The correlation coefficients of aerosol loading (contours in Figs. 4 and 5 (a1-a4)) in the well-mixed layer with the U_{10m} were added according to and referee 1's specific comment (42) and referee 2's minor comment (8).

(3) The global ocean data are used in the analysis of the factors controlling MBL decoupling structure and stratiform cloud top behaviors instead of eastern Pacific Ocean data according to referee 1's major comment (4). Related statements were revised accordingly based on the new results. Correlation coefficients and their significance levels were provided in the analyses according to referee 1's major comment (4), referee 2's main issue (1), and referee 3's comment (1).

Acknowledgements: Acknowledgements now include all the instrument teams and data providers as suggested by referee 1's specific comment (56) and referee 2's minor comment (9).

Figures: All figures were re-plotted according to reviewers' comments.

Language: All language issues from reviewers' comments were corrected as suggested (not listed here one by one). Efforts were made to improve the language of the manuscript and the paper was proofread by the OSA Language-Editing Service.

The detailed point-to-point responses are given below:

General response

The authors thank the reviewers for their helping to improve this manuscript and the English langrage. We greatly appreciate your detail comments and creative suggestions. We revised the paper according to your suggestions. Our replies to the comments are given below.

Anonymous Referee #1

Received and published: 15 December 2015

Review of "Marine boundary layer structure as observed by space-based lidar" by Luo et al. for publication in Atmospheric Chemistry and Physics.

The authors present an investigation of the marine boundary layer in the eastern Pacific, primarily during the MAGIC field campaign, but also extending to a 4 year (2006- 2010) climatology using the lidar on the CALIPSO satellite. They examine processes related to decoupling within the boundary layer resulting in a well-mixed layer within the deeper boundary layer structure. In addition to CALIPSO, they examine soundings from the field campaign, AIRS retrieved soundings, and estimates from ECMWF among others. Several issues with the analysis and description need to be addressed before publication in ACP.

Major comments

1) You specify that you do not use any cloudy CALIOP profiles in your estimation of BLH structure and this needs further clarification. Did you remove every profile affected by clouds or only those meeting some threshold? Did this include thin cirrus? How did you calculate MLH under these conditions?

Reply: In this paper, we used CALIOP profiles with no cloud below 8km, including cases with clouds above 8km. The MLH is calculated based on aerosol backscattering coefficient, which is not affected by the high clouds. Details were added into manuscript and relative statements in section 2 and section 3.2 were changed.

2) In your comparisons between MAGIC soundings and CALIOP, in order to be consistent, you should only examine clear-sky MAGIC soundings. Otherwise you are comparing different conditions. Also, you specify that the collocations are within 2.5 degrees, but you don't specify the time range. What temporal restrictions did you use for your collocations.

Reply: The evaluation of lidar methodology with soundings were performed with 2-year (2007-2008) clear-sky Atmospheric Radiation Measurement Program (ARM) Climate Research Facility (ACRF) radiosonde and micro pulse lidar (MPL) observations (Xie et al., 2010, Mather and Voyles, 2013) at Nauru (marine site). Compared to radiosonde-derived BLH, the bias and root mean square error (RMSE) of MPL derived BLH is -0.12 ±0.24 km and correlation coefficient between each other is 0.75. Compared to radiosonde-derived MLH, the bias and RMSE of MPL derived MLH is -0.06 ±0.16 km and correlation coefficient between each other is 0.66. Compared to radiosonde-derived MLH/BLH, the bias and RMSE of MPL derived MLH/BLH is -0.02 ±0.1 and correlation coefficient between each other is 0.61. All the correlation coefficients are reported at confidence level of 0.01. These evaluations indicate the good accuracies of our lidar based BLH and MLH determinations for clear-sky MBL structure study. Relative statements were added into this section.

The MAGIC soundings are mostly under cloudy conditions and are poorly collocated with CALIPSO overpass. The temporal restriction for the collocation is 1 day. The purpose of the evaluations of CALIOP with MAGIC soundings was to show that the CALIOP-observed clear-sky MBL structure could be similar to the structure of the nearby cloudy-sky MBL in some extent. This is the basic assumption for discussion in section 4.2. Relative statements were added into this section and section 4.2.

3) In general, parts of the analysis stating good correlation would greatly benefit from the authors providing correlation coefficients and a measure of the statistical significance.

In multiple sections, the authors state that two things are well correlated, but show no quantitative evidence, other than an examination of the plots which can be subjective, especially since some of the plots are small and hard to read.

Reply: The correlation coefficients and a measure of the statistical significance were provided in the analysis now when discussing their agreements. The plots were improved according to referees' comments.

4) In the conclusions, you state that MBL decoupling is mainly controlled by EIS, but I don't think you've shown this. If that were the case, I'd expect to see a stronger relationship between the two. In a global analysis (i.e. not just over eastern Pacific), I would like to see the correlation coefficients and their significance and an explanation of the physical mechanisms and why other variables (e.g. SST) are not responsible before making this claim. Correlation does not equal cause and effect.

Reply: Now, the analysis was performed over the global ocean, and the correlation and statistical significance were provided to show the relationship between EIS and MBL decoupling.

The entrainment of the dry warm air above the inversion can be the main factor controlling the MBL decoupling. The EIS has a significant control of the MBL top entrainment. Because the SST, wind shear and surface heat flux also affect the entrainment process (Venzenten et al., 1999), it is reasonable to expect that these parameters also impact MBL decoupling. However, we did not find significant relationship between MBL decoupling and U_{10m} or SST. Instead, we found that the MBL coupling structure is controlled by both LTS and EIS when EIS < ~3 K, that is, better mixed MBL with increasing of EIS and decreasing of LTS. One reason for a weak relationship with U_{10m} or SST could be the uncertainties in satellite retrievals of these parameters. Another reason could be that the role of other variables was partially included by the EIS and LTS. Statements were changed to reflect the above discussion.

5) Please proofread the English grammar more carefully.

6.1 **Reply:** We put efforts on the language and the paper was proofread by the OSA Language-Editing Service. The manuscript is improved now.

Specific comments:

1) The title implies that this analysis relies primarily upon space-based lidar when much of the analysis relies on data from other instruments. In section 3.2, it is stated that only BLH estimated from clear-sky CALIOP profiles are used. Considering that much of the analysis concerns the presence of stratocumulus and cumulus clouds, conditions in which CALIOP is not used, the title is misleading and should be changed to reflect the broader array of instrumentation used.

Reply: The title was changed to 'Marine Boundary Layer Structure as Observed by A-Train Satellites'.

2) Page 34066, line 19: "However, over oceans, the BLH is associated with the aerosol layer top (clear sky) or stratiform cloud top (cloudy sky), : : :" How does this differ from BLH and MLH over land?

Reply: As shown in Luo et al. (2014a), over land, the gradient or variance methods could identify the BLH, while aerosol layer top is usually higher than the BLH. The statement was added.

3) Page 340066, line 20: the word below is misspelled

Reply: Corrected.

4) Page 34066, line 21: You state that there is a strong aerosol gradient at the top of the MLH. Is this not present also at the BLH top? If not, how does your threshold method

detect the BLH?

Reply: The lidar methodology were developed and evaluated with the 2-year (2007-2008) clear-sky Atmospheric Radiation Measurement Program (ARM) Climate Research Facility (ACRF) radiosonde and micro pulse lidar (MPL) observations (Xie et al., 2010, Mather and Voyles, 2013) at Nauru (marine site). As detailed in Luo et al. (2014a), over ocean, the MBL top (BLH) is usually at the aerosol layer top, and the MLH is usually close to the height with a strong aerosol gradient below BLH. For decoupled MBL, the aerosol gradient at the BLH top is weaker than that at the MLH top, as a case shown in Figure 4 in Luo et al. (2014a). For well-mixed MBL, the BLH and MLH are same.

5) Page 34066, line 25: "Difficulties in identifying stratiform clouds: : :" Do you mean difficulties in differentiating between cumulus and stratiform clouds?

Reply: Changed to 'differentiating between cumulus and stratiform clouds'.

6) Page 34067, lines 17-19: The phrasing here is awkward. Please reword. Please also specify that the 532nm polarized backscatter is both perpendicular and parallel polarizations.

Reply: Rephrased to 'CALIOP is a dual-wavelength (532 and 1064 nm) backscatter lidar, which is carried on the Cloud-Aerosol Lidar and Infrared Pathfinder Satellite Observations (CALIPSO) (Winker et al., 2007; Winker et al., 2009). At 532 nm, the CALIOP provides both the parallel and perpendicular polarization components of attenuated backscatter.'

7) Page 34067, line 23: You need to introduce CloudSat (and later AMSR-E) and provide references.

Reply: Information of CloudSat and AMSR-E was added as suggested.

8)Page 34068, lines 9-11: The explanation of EIS could be clearer. Perhaps including the equation would be helpful. Also, what level moist adiabatic lapse rate did you use?

Reply: Equation was added. The moist adiabatic lapse rate is at 850hpa.

9) Page 34068, line 8: The text says you use the surface potential temperature, but the equation here implies 1000 hPa potential temperature. Which did you use?

Reply: The equation was changed to match the text.

10) Page 34068, lines 25-26: How do you differentiate between the AMSR-E passes in your analysis; which did you use? What is the timescale of these maps? Did you use daily data, monthly, etc.?

Reply: We used both ascending and descending passes for daytime and nighttime orbits. The AMSR-E passes were differentiated based on the geo-locations and observation times provided in this dataset. AMSR-E Level 3 daily Ocean Products version-7 was used. Information was added.

11) Page 34068: Specify that AMSR-E is onboard Aqua and therefore is collocated with AIRS and AMSU and in the A-train with CALIPSO and thus the instruments are sampling similar conditions and time of day.

Reply: Statements were added as suggested.

12) Page 34068, lines 26-27: You specify the RMS differences, but don't say relative to what. This information is necessary for understanding the associated uncertainty.

Reply: Statements were changed to 'Error in the data was estimated using the root mean square (RMS) difference between AMSR-E U_{10m} and U_{10m} coming from four other satellite microwave radiometers (three SSM/Is and TRMM TMI) and with U_{10m} from the satellite microwave scatterometer QuikScat (0.92 m/s with a bias of 0.57 m/s) (Wentz et al., 2003). This calculation gave an RMS difference between AMSR-E SST retrievals and the Reynolds SST as 0.76 K (Wentz et al., 2003). Validation using data from a buoy (National Data Buoy Center, NDBC) U_{10m} (mean value of 6.61 m/s) gave an RMS difference with AMSR-E U_{10m} (mean value of 6.46 m/s) is 1.63 m/s with a bias of −0.15 m/s (Luo et al., 2015). Validation with NDBC buoy SST (mean value of 299.49 K) in this study showed that the RMS difference in AMSR-E SST (mean value of 299.26 K) is 0.99 K with a bias of −0.23 K. '

13) Page 34069, line 1: Earlier, you state that AMSR-E data are on a 0.25 degree map, but here you say 25km. Which resolution is used?

Reply: Changed from 25km to 0.25 degree.

14) Page 34069, line 7: Spell out GPCI

Reply: Added.

15) Page 34070, lines 6-10: If the HSRL signal is negatively impacted by cloud cover and much of the transect included clouds, what uncertainty is present in your aerosol distribution estimate?

Reply: The HSRL signal was only used to show the aerosol and cloud vertical distribution along the transect. The HSRL can detect the aerosol signal below clouds because it is looking upward from ship. As can seen in Figure 1 when western than longitude of ~-140^{o}, there is a layer below clouds (if exist) with more aerosol loading and with the layer top close to the MLH identified from radiosonde. Due to the high cloud occurrence along MAGCI transect, we did not applied the lidar methodology to HSRL clear-sky profiles.

16) Page 34070, line 12: Why is sonde in all capital letters and why is radiosonde or rawinsonde not spelled out?

Reply: Changed 'SONDE' to 'radiosonde' throughout the manuscript.

17) Page 34070, line 22: Did you determine the method based on the structure? Please clarify or reword. Was the MLH detected by radiosonde or the lidar? If it was the

radiosonde, how was this determined?

Reply: Statement was removed.

The MLH was detected with both radiosonde and the lidar.

For radiosonde, MLH height was identified as the base of the first inversion layer with inversion strength larger than 0.05K/100m in radiosonde potential temperature profiles.

Statements were changed to make it clear.

18) Page 34070, line 23: "Figure 1 presents the one transect: : :" was there only one transect?

Reply: There are total 40 transects in MAGIC field campaign. Figure 1 presents one transect.

19) Page 34070, line 24: Temperature is misspelled. Please use spell check.

Reply: Corrected.

20) Page 34070, lines 24-25: What is the correlation between the BLH and aerosol layer/Sc top?

Reply: The correlation coefficient between the radiosonde BLH and aerosol layer top is 0.75 for clear-sky observations (at the ARM Nauru cite), and is 0.56 for loosely collocated clear-sky CALIOP and all-sky MAGIC observations. The correlation coefficient between the CALIOP-derived BLH and Sc top is 0.66. All correlation coefficients are at confident level of 0.01. Statements were added into this section.

21) Page 34070, lines 22-26: How close is the spatiotemporal location of the soundings with HSRL?

Reply: The soundings and HSRL were all deployed on the commercial cargo container ship Horizon Spirit in MAGIC field campaign.

22) Page 34071, line 2 and Fig. 1: It is difficult to see the inversion associated with the

MLH described in the text in this figure. It would be helpful to see one profile of theta with the associated TAB from HSRL.

Reply: The figure can be found in Figure 4 of Luo et al. (2014a) with ground-based lidar and radiosonde observations. Statement was added.

23) Page 34071, line 8: How was the 0.05K/100m threshold identified?

Reply: The threshold was chosen based on visual check through all MAGIC transects. Statement was added to clarify it.

24) Fig 1: What does it mean when the MLH in Fig. 1 is at the surface. To my eye, it looks like MLH=BLH east of longitude 137 degrees W.

Reply: The lower limit of the y-axis is 0.3km. The radiosonde-derived MLHs are ~0.3km due to weak inversion above this height when east of longitude 137 degrees.

25) Page 34071, line 23: Since the sonde data are not the truth, do not say that the CALIOP derived BLH are biased lower. Just say that they are lower. And this is not true over the eastern domain.

Reply: ‘biased’ was removed.

26) Page 34071, lines 25-26: How large is the spatial mismatch? What is the temporal mismatch? How many observations go into both estimates? A better comparison would limit the radiosonde data to clear-sky only so they are more comparable to the CALIPSO estimates.

Reply: We used quite loose constrains (1-day and 2.5 degree) to find collocated MAGIC and CALIOP measurements. However, the statistical results showed that the CALIOP-observed clear-sky MBL structure could capture a similar structure of the nearby cloudy-sky MBL.

The clear-sky only evaluation of the lidar methodology was added by using the 2-year (2007-

2008) collocated clear-sky Atmospheric Radiation Measurement Program (ARM) Climate Research Facility (ACRF) radiosonde and micro pulse lidar (MPL) observations (Xie et al., 2010, Mather and Voyles, 2013) at Nauru (marine site).

27) Page 34072, lines 1-4: Why would you expect a cloud-free regime and a cloudy regime to have similar BLH? And if the spatiotemporal mismatch is very large, such that one is not representative of the other, why is there good agreement?

Reply: Even though there are differences between a cloud-free regime and a cloudy region, but during MAGIC, we expect the both regimes show a consistent picture of MBL transition from the coastal to the far ocean. That is why they agree statistically but with small mean differences.

28) Page 34071, line 6: indicates is misspelled. Please use spell check.

Reply: Corrected.

29) Page 34071, line 6: LCL is shown in Fig. 2c, not 2b.

Reply: Corrected.

30) Page 34071, lines 10-12: What are the correlation coefficients for these comparisons? Are they statistically significant? For instance, the BLH seems to be an average of 1-1.5 km so an error of 25-40% seems large. What is your justification for this being a good fit?

Reply: Those were compared between CALIOP cloud-free cases with MAGIC cloudy cases based on loosely collocated data, which results in large random errors in the comparison. As mentioned above, data from the both regimes show a consistent trend. As given in the reply to your major comment 2, the comparison based on collocated cloud-free cases at an ARM tropical site was given to more reliably to show the performance of the algorithm.

31) Page 34072, line 16: How is the MBLC dataset built?

Reply: The MBLC dataset includes cloud type and stratiform-cloud top based on 2B-CLDCLDCLASS-LIDAR, and drizzle information based on 1B-CPR dataset as described in the previous section. The statement was changed to 'In this section, we will investigate the MBL structure over the eastern Pacific Ocean with the 4-year new MBL and marine boundary layer cloud (MBLC, including cloud type and stratiform-cloud top based on 2B-CLDCLDCLASS-LIDAR, and drizzle information based on 1B-CPR) dataset as described in the previous section.'

32) Page 34072, line 24: Cold SST could also be partly responsible. If it was due solely to subsidence, the BLH would be low over the deserts.

Reply: Changed to 'due to the strong subsidence and cold SST'.

33) Page 34072, line 26: How do you determine the clear-sky BLH when convection is occurring? Usually convection is associated with clouds.

Reply: The SST over the ITCZ region is high, which can result in stronger buoyancy-driven turbulence and thus stronger vertical mixing. Statement was changed to 'The BLH is high over the Intertropical Convergence Zone (ITCZ) due to large-scale convergence and the high SST, which results in strong buoyancy-driven vertical turbulence mixing' to make it clear.

34) Page 34073, lines 7-11: Please rephrase. First you say there are magnitude differences and then you provide an example where you say that McGrath-Spangler and Denning give a similar pattern and value. These two statements are inconsistent.

Reply: The BLH reported in McGrath-Spangler and Denning (2013) show a quite similar pattern and value to the MLH in our results, which means their BLH is much lower than the BLH in our results. Statements were changed to clear this point.

35) Page 34073, line 17: There is a minimum in MLH/BLH over the equator, implying weaker mixing from 160W to 100W

Reply: Statement was added.

36) Page 34073, lines 25-26: This is repetitive

Reply: Deleted.

37) Page 34073, lines 19-29: If clear-sky is included, how do you define a CTH in the case without clouds?

Reply: Within the collocated 0.25^o grid-box, there are many cases with the part of grid-box covered by stratiform clouds and the rest being clear sky. In these cases, both BLH and CTH are available and good correlation cloud be found between the BLH and stratiform CTH as shown section 3.2. Statement was added to clarify it.

38) Page 34073, line 27: What cloud types are away from the coast with tops _2.5km?

Please state to be consistent with your statement about stratiform clouds in the previous line.

Reply: 'the drizzled stratiform cloud tops' was added here.

39) Page 34074, line 1: Specify what you mean by "approaching the central Tropical

Pacific"

Reply: Changed to the tropic Pacific near longitude of ~180^{o}W.

40) Page 34074, lines 6-7: Are these stratiform clouds included in Fig. 3a?

Reply: The BLH and MLH were identified from the clear-sky CALIOP profiles in the collocated 0.25^o grid-box. Therefore, Fig. 3a includes all cases with cloud fraction <1.

41) Page 34074, lines 8-12: Reword to make clear that heterogeneous conditions are less likely to precipitate than more homogeneously cloudy ones.

Reply: Reworded as suggested.

42) Page 34074, line29: When you state something has a good positive correlation, please include the correlation coefficient and the significance.

Reply: The optical depth in the lower well-mixed layer has the correlation coefficient of 0.64 at confident level of 0.01 with the U_{10m} in NPO, but the correlation coefficient is -0.08 at confident level of 0.39 in the SPO. The statement was added.

43) Page 34075: There appears to be a seasonal cycle in the near coastal aerosol concentrations in the SPO transect. Can you comment on this?

Reply: The seasonal cycle in the near coastal aerosols is mainly driven by seasonal sea salt source (link with wind) and MLH and BLH variations. However, the near coastal aerosol can still be influenced by the continental aerosol sources.

44) Page 34075, line 12: "Sc occurrence and EIS correlate well: : :" this is not true near the coast. What other processes could be involved?

Reply: Other processes such as sea-land breeze and cold current near the coasts of Northern and Southern America resulting cold SST could be involved. Statements were added.

45) Page 34075, line 13: If drizzle occurrence isn't discussed other than to say it isn't correlated with EIS, why show it in this plot?

Reply: Removed from the plot.

46) Page 34075, line 25: This doesn't seem to be the case for NPO during DJF. Do you have any explanation for the seasonal dependence?

Reply: We further investigated the possible controlling factors to the $CTH_{no\ drizzle}/CTH_{drizzle}$ beyond EIS over global oceans. The SST was found to be important. Under cold SST (SST<~20°C), mean $CTH_{no\ drizzle}/CTH_{drizzle}$ does not vary with EIS. Under warm SST (SST>~20°C) where the Sc-to-Cu transition happens, the mean $CTH_{no\ drizzle}/CTH_{drizzle}$ shows good correlation with EIS, with the correlation coefficient >0.89 at confident level of 0.01.

The near-coast (eastern than ~-130) SST for NPO during DJF is close to or colder than 20^{o}C. Therefore, it seems no good relationship between EIS and $CTH_{no\ drizzle}/CTH_{drizzle}$ for this season.

Figure 6(c) and relative statements were changed.

47) Page 34076, lines 17-18: Please rephrase for clarity.

Reply: Rephrased as 'The $CTH_{no\ drizzle}$ is close to the BLH but is lower than the $CTH_{drizzle}$.'.

48) Page 34077, lines 19-21: If Sc represent more than 1/2 of the grid box and CALIOP has a small footprint, why would clear-sky MBL be represented in the average?

Reply: According to the evaluations of CALIOP-derived clear-sky MBL structure with MAGIC cloudy-sky MBL structure and the evaluation of CALIOP-derived clear-sky BLH with the nearby stratiform cloud top from 2B-CLDCLASS-LIDAR in section 3.2, it is reasonable to assume that the cloud-topped MBL can have the similar structure to the nearby clear-sky MBL within the 0.25° footprint for the Sc and Cu MBL cases. Statements were added.

49) Fig. 7: In Section 3.2, you say you cannot use CALIOP to estimate BL structure in cloudy conditions so what is your justification for using it to show TAB under stratiform and Cu conditions?

Reply: Figure 7 is the mean BL structure in term of TAB from the cases with both clear-sky and stratiform/Cu cloud in the same 0.25^{o} grid box. The definitions of the stratiform and Cu cloud conditions were in this section and in the caption of the figure. Relative statements were revised to make it clear.

50) Fig. 1 caption: The diamonds and circles are black, not magenta.

Reply: Corrected.

51) Fig. 2: Instead of showing the 1:1 line, it would be helpful to show a best fit line or

lines.

Reply: Due to uneven data samples the best-fit line may be misleading. Thus, we only provide related statistics in the text. The 1:1 line offers a simple way to assess differences between different measurements.

52) Fig. 3: I don't believe Fig. 3h (u10m) is discussed. If not, please remove.

Reply: Removed as suggested.

53) Fig 4: For consistency with Fig. 5 and to make it easier to determine proximity to the coast, change the x-axis to show longitude.

Reply: Changed as suggested.

54) Fig. 6: (1) Are these scatter plots? If so, please remove the connecting lines. (2) What instrument is used to calculate the MLH/BLH here (6b)? (3) Please label the y-axis in Fig. 6c.

Reply: (1) The lines were kept to make the trends in plots more clear.

(2) It is CALIOP-derived MLH/BLH in (6b). **A** statement was added to clarify it.

(3) Added.

55) Fig. 7: (1) Are these associated with a particular season or the 4 year climatology? (2) How many profiles are averaged in each? Are any cases better or worse sampled?

(3) If you're including BLH up to 1.6 km in Fig. 7c, extend the y-axis to include these values.

(4) Please include symbols to indicate the estimated BLH and MLH so your point is clear about decoupling between the two with varying EIS and BLH.

Reply: (1) These are the 4-year climatology. A statement was added to clarify it.

(2) The total case numbers in each plot are (a1) 7019; (a2) 903; (a3) 3050; (b1) 9911; (b2) 1595; (b3) 3900; (c1) 11166; (c2) 1714; (c3) 4249. The number of stratiform cloud case is smaller than other two cases, but is still large enough to support the statistical analysis (70-400 cases were averaged for each stratiform cloud case profile).

(3) The y-axis is extended to 2km.

(4) We tried to add symbols but the plots become too complicated. Also, these are mean profiles from individual profiles with different MLH. The BLH for (a1-a3) is ~ 0.7km, for (b1-b3) is ~1.1km, and for (c1-c3) is ~1.5km. The MLH varies profile by profile from ~0.5 to ~0.9km.

56) Your acknowledgements need to include the instrument teams and data providers. For instance, if you acquired the CALIPSO data from the ASDC, they provide a sample acknowledgement (available from https://eosweb.larc.nasa.gov/citing-asdc-data): Citing ASDC Data Acknowledgments The data obtained from the Atmospheric Science Data Center (ASDC) are free of charge for use in research, publications, and commercial applications. When data from the ASDC are used in a publication, we request this acknowledgment be included: "These data were obtained from the NASA Langley Research Center Atmospheric Science Data Center."

A lot of work goes into collecting and archiving the data that you used and this effort needs to be acknowledged. Additional acknowledgements are required for each of the datasets you used. Most data providers also provide a sample acknowledgement.

Reply: Acknowledgements were revised as suggested.

Anonymous Referee #2

The authors present a study of the boundary layer height and mixing layer height based on 4 years of CALIOP data using the clear sky aerosol backscatter in the eastern pacific region, with additional help from CLOUDSAT, AIRS, AMSR-E data and ECMWF model data. The use of the CALIOP data is evaluated using data from the MAGIC field campaign and SONDE data. The relation of the decoupling of the estimated boundary

layer height and mixing layer height with the estimated inversion strength is explored. The study shows a promising method of studying the boundary layer structure using satellite lidar data. I am very impressed with the BL dataset the authors have made using the CALIPSO data.

Many of the major issues have already been addressed by the Anonymous referee 1, I will not add them here again.

(1) The main issue I want to mention here is that the authors need to add correlation values, and in some cases the means/rms (see below) when they are discussed. The results discussed can only be appreciated and referred to in future work when we can assess the real values/effects.

Reply: Thanks for the comments. We have added correlation values, significant level, and in some cases the means/rms in the revised manuscript.

Minor additional comments:

(1) Please use spell checker once more! Page 34065 Lines 4-11: Please rephrase the entire paragraph, each individual line is short and uses the word decoupled making it hard to read.

Reply: We put efforts on the language and the paper was proofread by the OSA Language-Editing Service. The manuscript is improved now.

Rephrased as suggested.

(2) Page 34066: line 20 bellow ! below

Reply: Corrected.

(3) Page 34068: lines 26-27. The RMS of the SST can be seen as relatively small knowing roughly the absolute mean values but in case of the winds it is hard to see if the bias and rms are high or low. Please provide the mean values for both wind and sst. Are the RMS and bias in the wind absolute or relative to the wind value, i.e. is the rms for all winds representative of the error or is it overestimated by the occurrence of a few higher wind events?

Reply: There are no mean values reported in Wentz et al. (2003). Validations of AMSR-E SST and U_{10m} with NDBC bouy SST and U_{10m} were added in to this paragraph.

Statements were changed to '**Error in the data was estimated using the root mean square (RMS) difference between AMSR-E U_{10m} and U_{10m} coming from four other satellite microwave radiometers (three SSM/Is and TRMM TMI) and with U_{10m} from the satellite microwave scatterometer QuikScat (0.92 m/s with a bias of 0.57 m/s) (Wentz et al., 2003). This calculation gave an RMS difference between AMSR-E SST retrievals and the Reynolds SST as 0.76 K (Wentz et al., 2003). Validation using data from a buoy (National Data Buoy Center, NDBC) U_{10m} (mean value of 6.61 m/s) gave an RMS difference with AMSR-E U_{10m} (mean value of 6.46 m/s) is 1.63 m/s with a bias of −0.15 m/s (Luo et al., 2015). Validation with NDBC buoy SST (mean value of 299.49 K) in this study showed that the RMS difference in AMSR-E SST (mean value of 299.26 K) is 0.99 K with a bias of −0.23 K. '

The RMS and bias in the wind are absolute values.

(4) Page 34070 ; Lines 8-10. The method was not used, did you estimate the MBL on any

other way or was this not possible at all. And if not, what did you do with the data of the cloud contaminated data, since you mention in 34071 line 22 that the MHL was based on the MBL structure observed in MAGIC

Reply: The CALIOP-based MBL structure identification method was only applied to the cloud-free CALIOP profiles by using the aerosol vertical distribution as the proxies of BLH and MLH. For cloudy conditions, the CALIOP cannot penetrate the thick cloud to detect the aerosol below clouds, and the stratiform cloud top was treated as the MBL top in this paper.

To evaluate the CALIOP-based MBL structure, MAGIC soundings were used to determine the MBL structure. Due to the high occurrence of the cloud along the MAGIC transect (as can be seen in figure 1), we did not apply the CALIOP-based MBL structure identification method to the ship-based HRSL observations.

Line 13: What does SONDE stand for. Do you mean Sonde or is it an abbreviation not defined.

Reply: Changed to 'radiosonde'.

(5) Page 34071: Line 23. Biased lower is not correct here. That would mean that SONDE is the truth.

Reply: Changed 'biased lower' to 'lower'.

(6) Page 34072: Line 4/5 please provide correlation values. The red dots in Figure 2 show

no correlation in this presentation, a 2D histogram may show that there is a positive correlation but not as plotted here. Same holds for Lines 10/11. To strengthen your case you should provide a correlation factor (the figure does show this of course in 2d)

Reply: The correlation values were added as suggested.

Line 15 ‘’built in the last” ! described in the previous

Reply: Changed as suggested.

(7) Page 34073: Line 2 : correct “shows increase tendency when westwards”

Reply: Changed to ‘shows westward increasing tendency’.

Line 11: results

Reply: Corrected

(8) Page 34074 Discussion on salt aerosol vs U10 in NPO and SPO. I am not convinced by the explanation of the lack of U10 correspondence in the SPO region. Could you compare the TAB vs U10 along the two boxes. This way you may be able to see if above a MLH threshold value the NPO and SPO show the same U10-TAB[for Z< ZBLH] relationship.

Reply: We have examined the relationship between sea salt aerosol optical depth and U10. The optical depth in the lower well-mixed layer has the correlation coefficient of 0.64 at confident level of 0.01 with the U_{10m} in NPO, but the correlation coefficient is -0.08 at confident level of 0.39 in the SPO. Statements were added.

(8) Page 34076 Lines 9-13 Give values of mean/error and correlations when you mention it in the discussion

Reply: The correlations were added in the discussion. The errors were added into figure 6 and its caption.

(9) Acknowledgements: You use a lot of data sources but mention non of these in the acknowledgements. Please add those from which you downloaded the data (i.e. MAGICS/calipso/SONDE)

Reply: Changed as suggested.

Figures:

(11) Figure 1 Change Magenta to Black

Reply: Changed.

(12) Figure 3: Skip a number of latitude values, it feels crowded

Reply: Changed as suggested.

(13) Figure 4/5: Small fonts. EIS values unreadable as they overlap vertically, lower text of CTHxx in d3 and d4

Reply: The figure was re-plotted to make the text clear.

(14) Figure 6a: Provide error estimates in Figure to provide a visual estimate of what we look at and if the slope difference has significance. You can also show it in a contour lightly colored box if you are afraid that it becomes crowded

Reply: Error was added into plot and was stated in figure caption.

Anonymous Referee #3

Received and published: 31 December 2015

This paper uses clear sky aerosol back scattering signal to estimate boundary layer height (BLH) and mixing layer height (MLH) and then studies the relation between MBL decoupling (MLH/BLH) and the estimated inversion strength (EIS). The overall research topic is interesting and approach is good. However, the analysis needs to be more quantitative and there should be more descriptions on the data processing. I would be happy to recommend the publication of this paper when the following concerns are addressed.

1) Provide quantitative measures whenever possible. I list here a few examples for reference. The uncertainties in the estimated BLH and MLH using the aerosol back scattering are estimated by comparing with SONDE-derived heights. (See first paragraph in page 34071.) But, for MLH, is +/-0.45km a good precision? How would it affect the relation between the ratio BLH/MLH and EIS? For fig 2b, it would be useful to report also the correlations between SONDE and CALIPSO-derived heights to tell how tightly the heights derived by SONDE and CALIPSO are connected.

Reply:

The MAGIC soundings are mostly under cloudy conditions and are difficult to be collocated with CALIPSO overpass. Thus, we have to relax the temporal difference for the collocation to 1-day. Therefore, the large spatial and temporal separations result in large differences between the two measurements. The main purpose of the evaluations of CALIOP with MAGIC soundings was to show that the CALIOP-observed clear-sky MBL structure could be similar to the structure of the nearby cloudy MBL in some extent. This is the basic assumption for the discussion in section 4.2. Statements were added to make the points more clear now.

To better evaluate the lidar-base MLH and BLH detection with radiosonde measurements, we analyzed 2-year (2007-2008) collocated clear-sky Atmospheric Radiation Measurement Program (ARM) Climate Research Facility (ACRF) radiosonde and micropulse lidar (MPL) observations (Xie et al., 2010, Mather and Voyles, 2013) at Nauru (marine site). Compared to radiosonde-derived BLH, the bias and root mean square error (RMSE) of MPL derived BLH is -0.12 ±0.24 km and correlation coefficient between each other is 0.75. Compared to radiosonde-derived MLH, the bias and RMSE of MPL derived MLH is -0.06 ±0.16 km and correlation coefficient between each other is 0.66. Compared to radiosonde-derived MLH/BLH, the bias and RMSE of MPL derived MLH/BLH is -0.02 ±0.1 and correlation coefficient between each other is 0.61. All the correlation coefficients are reported at confidence level of 0.01. These evaluations indicate the good accuracies of our lidar based BLH and MLH determinations for clear-sky MBL structure study. Relative statements were added into this section. These new evaluation results were added into this section.

In fig 3, it is also useful to use spatial correlations to quantify similarity between patterns.

Reply: The correlation coefficient between MLH and BLH is 0.6 at confidence level of 0.01 in spatial pattern. The correlation coefficient between stratiform cloud occurrence and EIS is 0.78 at confidence level of 0.01 in spatial pattern. The correlation coefficient between non-drizzled stratiform cloud top and the drizzled stratiform cloud top is 0.53 at confidence level of 0.01 in spatial pattern. Relative statements were added.

In fig 4,5, correlations with wind and EIS should be quantified.

Reply: The EIS over NPO shows negative correlation with the U_{10m}, with the correlation coefficient of -0.64 at confidence level of 0.01, but shows positive correlation with the U_{10m} when EIS <3 K over SPO, with the correlation coefficient of 0.6 at confidence level of 0.01. A statement was added.

In fig 6, the uncertainties of MLH/BLH, and EIS should be quantified.

Reply: Errors was added into the plot and into the figure caption.

2) provide more details about data processing. Here are some examples. For fig 3c, when computing MLH/BLH, is it computed as the ratio of average MLH and average BLH or the average of ratio over the 4 year? Is EIS only computed for clear sky? How do we connect with cloud, for example, in the discussion of last paragraph in page 34073?

Reply: Figure 3c is computed with the average of ratio over the 4 year.

The AIRS-derived EIS can only be obtained under clear-sky and broken cloud cover conditions. However, as shown in Yue et al. (2001), AIRS can provide reasonable the seasonal mean EIS as compared to model simulations and the AIRS-derived-EIS has strong connection with low cloud. It can also be seen in Figs. 3 that the correlation coefficient between the spatial distributions of stratiform cloud occurrence and EIS is 0.78 at confidence level of 0.01. A relative statement was added.

For fig 6, how are data points computed? Are they time averages of data at different spatial locations?

Reply: For Fig. 6 (a) and (b), there is no time averages of data, and data was sorted and averaged into different bins of EIS or LTS.

For Fig. 6 (c), data was averaged into 2.5-degree grid-box to provide seasonal means. Then the seasonal-mean data was sorted and averaged into different bins of EIS.

Details were added into the manuscript now.

Marine Boundary Layer Structure as Observed by A-train Satellites

Tao Luo, Zhien Wang, Damao Zhang and Bing Chen

University of Wyoming, Dept. Atmospheric Science, Laramie, WY, USA

Correspondence to: Z. Wang (zwang@uwyo.edu)

Abstract

The marine boundary layer (MBL) structure is important to the marine low cloud processes, and the exchange of heat, momentum, and moisture between oceans and the low atmosphere. This study examines the MBL structure over the eastern Pacific region and further explores the controlling factors of MBL structure over the global oceans with a new 4-year satellite-based dataset. The MBL top (BLH) and the mixing layer height (MLH) were identified using the MBL aerosol lidar backscattering from the CALIPSO (Cloud-Aerosol Lidar and Infrared Pathfinder Satellite Observations). Results showed that the MBL is generally decoupled with MLH/BLH ratio ranging from ~0.5 to ~0.8. The MBL decoupling magnitude is mainly controlled by estimated inversion strength (EIS), which in turn controls the cloud top entrainment process. The systematic differences between drizzling and non-drizzling stratocumulus tops also show dependence on EIS. This may be related to the meso-scale circulations or gravity wave in the MBL. Further analysis indicates that the MBL shows a similar decoupled structure for clear sky and cumulus cloud-topped conditions, but is better mixed under stratiform cloud breakup and overcast conditions.

7 Introduction

The planetary boundary layer is the lowest part of the troposphere that is directly influenced by the Earth's surface. It is considered to be important for the exchange of heat, momentum, and moisture between the surface and the upper troposphere (Stull, 1988). Over oceans, the marine_boundary_layer (MBL) clouds are frequently present within the MBL, making significant contributions to the energy and moisture budgets of the earth because of their high albedo (Klein and Hartmann, 1993; Norris and Leovy, 1994; Norris, 1998; Wood and Bretherton, 2004). Despite decades of research efforts, the MBL clouds are still one of the primary contributors to the uncertainty in the model predictions of climate change (Bony and Dufresne, 2005; Randall et al., 2007; Wyant et al., 2015). Because of the close interactions of MBL clouds with the vertical structure and turbulence of the MBL, the representation of convection and MBL processes is critical to the successful climate simulations (Randall et al. 1985; Albrecht et al., 1995; Bony and Dufresne, 2005; Wyant et al., 2010; Zhang, et al., 2011).

The decoupling of the MBL is frequently observed at the downwind of the subtropical stratocumulus regions when the turbulence does not strong enough to maintain a well-mixed MBL, especially when the MBL is higher than 1km (Bretherton and Wyant, 1997; Wood and Bretherton, 2004; Jone et al., 2011; Caldwell et al., 2012). A wide range of factors controls the MBL decoupling. Bretherton and Wyant (1997) suggested that the decoupling structure is mainly driven by an increasing ratio of the surface latent heat flux to the net radiative cooling in the cloud and that other factors such as drizzle, the vertical distribution of radiative cooling in the cloud, and sensible heat fluxes, only play less important roles. Meanwhile, Zhou et al. (2015) showed that the entrainment of the dry warm air above the inversion could be the dominant factor triggering the systematic decoupling, while surface latent heat flux, precipitation, and diurnal circulation did not play major roles.

The MBL structure and processes are still not well understood with observations mainly limited to specific case studies in early studies (Wood and Bretherton, 2004). The boundary layer structure can be derived from ground-based observations such as sounding (Seidel et al., 2010) or lidar (Emeis et al. 2008). However, ground-based observations of the MBL over the global oceans are sparse and may be not representative. Wood and Bretherton (2004) were the first to attempt a combination of MODIS and reanalysis data to study the MBL decoupling, though this passive remote sensing cannot produce direct measurements of MBL structures.

New satellite-based observations allow innovative ways to observe the boundary layer structure. The global boundary layer height (BLH) climatology has been derived by using Global Positioning System radio occultation (GPS-RO) measurements (Ratnam and Basha, 2010; Guo et al, 2011; Ao et al, 2012), the Lidar In-space Technology Experiment (LITE) (Randall et al., 1998), the Geoscience Laser Altimeter System (GLAS) (Palm et al., 2005), and the Cloud-Aerosol Lidar with Orthogonal Polarization (CALIOP) (Jordan et al., 2010, McGrath-Spangler and Denning, 2012, 2013). GPS-RO provides a valuable global view of height-resolved refractivity or moisture structure of boundary layer, but suffers with very coarse spatial resolutions (200 m in vertical and ~200 km horizontal) and has limited penetration into the lowest 500 m of the atmosphere (Xie et al, 2012). Satellite-based lidar is sensitive to boundary layer aerosols and clouds, providing global measurements of aerosol properties and their vertical distributions. As the aerosol vertical distribution in the boundary layer is heavily influenced by the boundary layer thermal structure, aerosol structures were used as a good proxy to study the MBL structures (Stull and Eloranta, 1984; Boers et al., 1984; Melfi et al., 1985; Boers and Eloranta, 1986; Leventidou et al., 2013; Luo, et al., 2014a; Kong and Fan, 2015).

Early studies have shown that satellite-based lidar is effective at deriving global BLH distributions (Randall et al., 1998; Palm et al., 2005; Jordan et al., 2010; McGrath-Spangler and Denning, 2012, 2013). This is especially true when using CALIOP observations, because of their much finer vertical (30m) and horizontal resolution (333m) in the lower troposphere. The aforementioned studies used gradient or variance methods over land and ocean under all-sky or no-optically-thick-cloud conditions. Over land, the gradient or variance methods could identify the BLH, which is usually lower than the aerosol layer (Luo et al., 2014a). However, over oceans, the BLH is associated with the aerosol layer top (clear sky) or stratiform cloud top (cloudy sky). Under decoupled MBL conditions, a well-mixed layer usually exists below the BLH with a stronger gradient in aerosol loading near the mixed layer height (MLH) than near the BLH (Luo, et al., 2014a). Thus, the aforementioned studies have the potential to report MLH as BLH as they did not fully consider the MBL decoupled structure in choosing lidar methodologies. In the MBL, difficulties in differentiating between the stratiform clouds and cumulus clouds could lead to BLH uncertainties, as the cumulus cloud top heights are often higher than the BLH. Those issues could result in statistical biases in marine BLH distributions differences in reported values and spatial distributions of the BLH over ocean among early studies.

After considering the MBL decoupling structure, a new CALIOP based approach was developed to reliably determine BLH and MLH in order to investigate the clear-sky MBL decouple structure (Luo, et al., 2014a). This study uses this new method to investigate the MBL decouple structure over the eastern Pacific Ocean region using CALIOP observations, and combining CloudSat observations with reliable cloud type identification to provide BLH information under stratiform-cloud-topped conditions. The authors also present an examination of the dependence of the MBL decoupled structure on environmental parameters over global oceans. Section 2 describes the data used in this study. Section 3 introduces and evaluates the lidar MBL structure identification methodology with the ship-base observations. Section 4 presents the results and discussions, and brief conclusions are in section 5.

8 Data

8.1 Satellite Observations and Data Collocation

This study uses multiple remotely sensed and operational meteorological datasets over global oceans during the period from June 2006 to December 2010.

Clear-sky MBL structure was determined from the cloud-free CALIOP measured aerosol backscattering with the cloud-free condition defined as no cloud below 8km, although cases with optically thin high clouds above 8km are included. CALIOP is a dual-wavelength (532 and 1064 nm) backscatter lidar, which is carried on the Cloud-Aerosol Lidar and Infrared Pathfinder Satellite Observations (CALIPSO) (Winker et al., 2007; Winker et al., 2009). At 532 nm, the CALIOP provides both the parallel and perpendicular polarization components of attenuated backscatter. The along-track footprint of CALIOP is 333m with the vertical resolution of 30m below 8.2 km. CALIOP level 1B data provide three calibrated and geo-located lidar profiles of 532nm and 1064nm total attenuated backscatter (TAB) and 532nm perpendicular polarization component. The molecular backscattering was estimated using the temperature and pressure profiles from the ECMWF-AUX (European Center for Medium range Weather Forecasting AUX-algorithm, Partain, 2004).

CloudSat carries a 94 GHZ cloud profiling radar (CPR) (Stephens et al., 2002). The CloudSat antenna pattern provides an instantaneous footprint at mean sea level of approximately 1.3 km, while vertically it has 125 bins with a bin size of about 240m. Cloud top height (CTH) and cloud type were obtained from the 2B-CLDCLASS-LIDAR product (Wang et al., 2012; Sassen and Wang 2012) with combining CloudSat and CALIOP observations, allowing better identify the cloud boundaries. In order to produce clear-sky aerosol information, cloudy CALIOP profiles were removed from further averaging. And the cloudy BLH was estimated from the CTH of marine stratiform clouds, which was a good proxy for estimating the marine BLH under cloudy conditions and has been widely used in the previous studies (Minnis et al. 1992; Wood and Bretherton 2004; Ahlgrimm and Randall 2006; Zuidema et al. 2009; Karlsson et al., 2010). Classification of drizzle within the Cloudy MBL was performed by applying a threshold of -20 dB (Leon et al., 2008) to the CloudSat CPR measured reflectivity factor in CloudSat 1B-CPR product (Tanelli et al., 2008).

The atmospheric large-scale stability parameters used in this study include lower tropospheric stability (LTS) (Klein and Hartmann 1993), and estimated inversion strength (EIS) (Wood and Bretherton 2006). LTS is calculated using the difference in potential temperature between 700 hPa and the surface ($\theta_{700} - \theta_{surface}$), whereas EIS is the difference between LTS and $\Gamma_{850} * (Z_{700} - LCL)$, where, Γ_{850} is the moist adiabatic lapse rate at 850hPa, LCL is lifting condensation level, and Z_{700} is the height at 700hPa. EIS is considered a more precise measure of the strength of a possible inversion than the LTS. EIS and LTS were estimated from AIRS (the Atmospheric Infrared Sounder) level 2 version 5 products (Jason, 2008). AIRS is a grating spectrometer carried on Aqua. It has a spectral resolution of $\nu/\Delta\nu \approx 1200$, a total of 2378 channels in the range of 3.7–15.4 μm with a few spectral gaps, and provides well-calibrated level 1B radiances (Overoye, 1999). AIRS is co-registered with AMSU (Pagano et al., 2003; Lambrigtsen and Lee, 2003), and the combined measurements are used to retrieve temperature, humidity and numerous other surface and atmospheric parameters. Geophysical retrievals are obtained in clear sky and broken cloud cover through the use of a cloud-clearing methodology (Susskind et al., 2003). Though there is no retrieval under overcast conditions, AIRS can provide a reasonable measure of the seasonal mean EIS as compared to model simulations (Yue et al., 2001). Additionally, the AIRS-derived EIS has strong connection with low cloud (Yue et al., 2001), making the, seasonal-mean EIS appropriate for the analysis of the MBL cloud behaviors in this paper.

The sea surface temperature (SST) and surface wind speed at 10m (U_{10m}) were obtained from AMSR-E Level 3 daily Ocean Products version-7 (Wentz et al., 2014). The Advanced Microwave Scanning Radiometer - Earth Observing System (AMSR-E) is a twelve-channel, six-frequency, passive-microwave radiometer system (Kawanishi et al, 2003). It measures horizontally and vertically polarized brightness temperatures at 6.9, 10.7, 18.7, 23.8, 36.5, and 89.0 GHz. Spatial resolution of the individual measurements varies from 5.4 km at 89 GHz to 56 km at 6.9 GHz. AMSR-E is co-located with AIRS and AMSU onboard Aqua and in the A-train with CALIPSO; thus, the instruments are sampling similar conditions and the same time of day. The daily AMSR-E Ocean Products are produced by Remote Sensing Systems (RSS, http://www.remss.com/). The orbital data is mapped to 0.25° grid box and is divided into 2 maps based on ascending and descending passes for daytime and nighttime orbits. Error in the data was estimated using the root mean square (RMS) difference between AMSR-E U_{10m} and U_{10m} coming from four other satellite microwave radiometers (three SSM/Is and TRMM TMI) and with U_{10m} from the satellite microwave scatterometer QuikScat (0.92 m/s with a bias of 0.57 m/s) (Wentz et al., 2003). This calculation gave an RMS difference between AMSR-E SST retrievals and the Reynolds SST as 0.76 K (Wentz et al., 2003). Validation using data from a buoy (National Data Buoy Center, NDBC) U_{10m} (mean value of 6.61 m/s) gave an RMS difference with AMSR-E U_{10m} (mean value of 6.46 m/s) is 1.63 m/s with a bias of −0.15 m/s (Luo et al., 2015). Validation with NDBC buoy SST (mean value of 299.49 K) in this study showed that the RMS difference in AMSR-E SST (mean value of 299.26 K) is 0.99 K with a bias of −0.23 K.

All the related datasets were collocated into AMSR-E 0.25° grid-box and cloud-free CALIOP backscattering profiles are then averaged. CALIOP backscattering profiles with no cloud below 8km (including cases with clouds above 8km) were averaged. Thus, within each 0.25° grid-box, there are three general conditions of the MBL: 100% cloud cover, partial cloud cover, and cloud-free. For the 100% cloud cover the BLH is determined from stratiform CTH. For the partial cloud cover, and cloud-free conditions the daily day- or night- averaged cloud-free CALIOP measurements are used to determine BLH and MLH. The following analyses only present data taken over the oceans (within 50°N and 50°S, and at least 200km away from continental boundaries), but include both daytime and nighttime observations. The MBL aerosol identifications are the same as in Luo et al. (2014a).

8.2 MAGIC and Collocated Satellite Observations

The Marine ARM GPCI (GCSS Pacific Cross-section Intercomparison, a working group of GCSS; GCSS is GEWEX Cloud Systems Study) Investigation of Clouds (MAGIC) field campaign (http://www.arm.gov/sites/amf/mag/) deployed the U.S. Department of Energy

(DOE) Atmospheric Radiation Measurement Program Mobile Facility 2 (AMF2) on the commercial cargo container ship Horizon Spirit from October 2012 through September 2013 with 20 round trips (Lewis et al., 2012; Zhou et al., 2015). The MAGIC transect is the line from the coast of California to Hawaii (35.8°N, 125.8°W to 18°S, 173.8°W) and was undertaken to provide unprecedented, intra-seasonal, high-resolution ship-based observations in order to improve the understanding of the Sc-to-Cu (Stratocumulus-to-Cumulus) transition along this transect. The AMF2 contained a state-of-the-art instrumentation suite and was designed to operate in a wide range of climate conditions and locations, including shipboard deployments.

This study used atmospheric soundings and MARMETX (marine meteorological measurements) datasets to characterize MBL structure. Standard radiosondes (Vaisala model MW-31, SNE50401) were launched every 6-hour to measure vertical profiles of the thermodynamic state of the atmosphere (temperature, pressure, relative humidity, and wind speed and direction). The MARMETX dataset (http://www.arm.gov/campaigns/amf2012magic/) contains standard surface meteorological parameters measured by the MARMET: temperature (T), pressure (P), relative humidity (RH), and apparent and true wind speed and direction; and the sea surface skin temperature measured by the Infrared Sea surface Temperature Autonomous Radiometer (ISAR) with an accuracy of better than 0.18°C.

The high spectral resolution lidar (HRSL, Shipley et al., 1983; Piironen and Eloranta, 1994) measuring total attenuated backscattering was also used to document the aerosol and cloud distributions. Because of the high occurrence of the cloud along the MAGIC transect, the lidar-based MBL structure identification method was not applied to the HRSL observations.

To evaluate the satellite-retrieved MBL structure with results from MAGIC soundings, the cloud-free CALIOP observations within a 2.5° grid-box and within 1 day of MAGIC soundings during October 2012 through September 2013 were collocated. The loose restriction was applied in the collocation, because limited MAGIC soundings, poor spatial coverage of CALIOP measurements, and high occurrence of clouds in the region. The cloud-free CALIOP profiles were firstly averaged into 0.25° grid-box to improve the signal-to-noise ratio. Then the MBL structure were identified and averaged into the 2.5° grid-box.

9 MBL Structure Identification Methodology

9.1 MBL structure identification methodology for radiosonde

For radiosonde, the BLH was determined by the Richardson number (RI) method (with the Eq. (2) in Vogelezang and Holtslag, 1996). This method determines the BLH as the height at where RI is larger than the critical value (= 0.25). The RI method is suitable for both stable and convective boundary layers. This method gives the BLH more physical meaning as it relates the derived BLH to boundary layer processes - surface heating, wind shear and capping inversion. Also, RI method does not produce a negative BLH, as it does not depend strongly on the sounding vertical resolution of the sounding. Therefore, the RI method is often considered as the best estimation against which to evaluate lidar based BLH estimations (Hennemuth and Lammert, 2006; Seidel et al, 2010).

Figure 1 presents one transect HSRL and potential temperature from MAGIC measurements. It is clear that the BLHs from the RI method correspond well with the aerosol layer tops, or stratiform clouds tops over the stratiform cloud region (eastern than longitude of ~-137^o). There is also some correspondence of BLHs with the highest cumulus clouds tops over the cumulus cloud region (western than longitude of ~-137^o). Over the cumulus cloud region the MBL becomes obviously decoupled, and there is usually one or more weak inversion layers below the RI determined BLH. The lowest inversion layer usually limits the upward transportation of the aerosols to form a layer, forming a layer with more concentrated aerosols than that above (this can also be seen in Figure 4 in Luo et al. (2014a)). This inversion can also limit the vertical developments of the small cumulus clouds that may form in the mixing layer. This characteristic allows the identification of MLH height as the base of the lowest inversion layer with inversion strength larger than 0.05K/100m in radiosonde potential temperature profiles. This threshold was chosen based on visual check of all MAGIC transects.

9.2 MBL structure identification methodology for CALIOP

As detailed in Luo et al. (2014b), the BLH can be determined with an improved threshold method using a threshold $\beta'_{thr} = \beta'_m + 2 * MBV$ applied to the marine aerosol backscattering coefficient profile retrieved from collocated CALIOP level 1B data. In this equation, β'_m is the molecular backscattering coefficient, estimated by temperature and pressure profiles from

ECMWF-AUX products; MBV is the measured backscatter variation, estimated as the standard deviation of measured attenuated backscatter coefficients from 30 to 40 km.

The MLH was identified by the gradient method (Luo et al., 2014a). The gradient of aerosol backscattering coefficient is calculated after three points moving average smoothing. After smoothing, the MLH is determined to be the lowest point with an aerosol backscattering coefficient gradient larger than 2 times of the molecular backscattering gradient.

The evaluation of lidar methodology with radiosonde soundings were performed with 2-year (2007-2008) clear-sky Atmospheric Radiation Measurement Program (ARM) Climate Research Facility (ACRF) radiosonde and micro pulse lidar (MPL) observations (Xie et al., 2010, Mather and Voyles, 2013) collected from Nauru (marine site). Detailed data process can be found in Luo et al. (2014a). When compared to radiosonde-derived BLH, the bias and root mean square error (RMSE) of MPL derived BLH is -0.12 ± 0.24 km with a correlation coefficient of 0.75. When compared to radiosonde-derived MLH, the bias and RMSE of MPL derived MLH is -0.06 ± 0.16 km with a correlation coefficient of 0.66. An overall comparison of radiosonde-derived to MPL derived MLH/BLH produces a bias and RMSE of -0.02 ± 0.1 and a correlation coefficient between of 0.61. All the correlation coefficients are reported at confidence level of 0.01. These small values of mean bias indicate that our CALIOP based BLH and MLH determinations for clear-sky MBL can be considered accurate.

Further evaluations were performed with loosely collocated CALIOP and MAGIC observations. While only cloud-free CALIOP profiles can be used to derive the MBL structure, the soundings were measured in all-sky conditions (mostly cloudy conditions) (Fig. 1). Figure 2 shows the comparisons of MBL structure between radiosonde and CALIOP measurements. The mean MBL structure by CALIOP and radiosonde along the MAGIC transect is shown in Fig. 2 (a). Both results show a similar trend in the MBL structure, being less decoupled near the coast and more decoupled over the far ocean. The heights of the CALIOP-derived BLH and MLH are lower than those derived from the radiosonde. Over the stratiform cloud regions, the CALIOP-derived MBL structure appears more decoupled than in the radiosonde results. However, the CALIOP-derived BLH shows good agreement with those from radiosonde as shown in Fig. 2 (b). The bias and RMSE in CALIOP-derived BLH were calculated to be -0.14 ± 0.37 km, with a correlation coefficient of 0.56 at the confidence level of 0.01. For CALIOP-derived MLH, the bias and RMSE is -0.1 ± 0.45 km with a correlation coefficient of 0.34 at the confidence level of 0.01. Although the biases are small, the RMSE differences are large, mainly as a result of limited sampling and large spatial mismatch, and different cloud conditions. This is especially true over the stratiform cloud region where the cloud fraction in the MBL is very high (Fig. 1). In this area the collocated cloud-free CALIOP profiles are often too far from the sounding observations to produce a strong correlation. However, Fig. 2 clearly shows that the CALIOP-observed clear-sky MBL structure captures a similar spatial trend as those from the nearby cloudy-sky MBL.

Additionally, the radiosonde-derived MLH agrees well with the LCL (Fig. 2(b)), with the bias and RMSE of -0.13 ± 0.21 km, and with a correlation coefficient of 0.73 at the confidence level of 0.01. Figure 2(d) shows that the CALIOP-derived BLH and stratiform CTHs (CTH_{sc}) within the same AMSR-E grid box over the eastern Pacific Ocean region show good agreements, with the bias and RMSE of -0.06 ± 0.52 km, and with a correlation coefficient of 0.66 at the confidence level of 0.01. Good agreement between the CALIOP-derived BLH and CTH_{sc} can also be found over the global oceans (Luo et al., 2014a).

10 Results and Discussions

10.1 MBL Structure over the Eastern Pacific Ocean

This section uses the 4-year new MBL and marine boundary layer cloud (MBLC) dataset described in the previous to investigate the MBL structure over the eastern Pacific. The MBLC dataset includes cloud type and stratiform-cloud (Sc) top and drizzle information based on the CloudSat products. Figure 3 shows the 4-year mean MBL structure (BLH, MLH and MLH/BLH), CTH_{sc} (with or without drizzle), EIS and U_{10m} over the eastern Pacific Ocean. Hereafter, the MBL structure (BLH, MLH and MLH/BLH) is referred to the clear-sky condition with aerosols as a proxy, while the CTHsc is used as the proxy of BLH under cloudy conditions.

The 4-year mean BLH over the eastern Pacific Ocean is shown in Fig. 3 (a). Fig. 3 (a) shows that the marine BLH is lower than ~1 km near the coast region at latitude of ~±30°. This is assumed to due to the strong subsidence and low SST. When moving away from the strong subsidence region, the BLH increases. The BLH is highest over the Intertropical Convergence Zone (ITCZ) attributed to large-scale convergence and the high SST causing strong buoyancy-driven vertical turbulence mixing. This is especially prevalent over the eastern Pacific near the Central America. However, the BLH is low along the equator with a tendency to rise heading westward. The 4-year mean MLH (Fig. 3(b)) shows a similar spatial pattern as the BLH, with a correlation coefficient of 0.6 at confidence level of 0.01. The rising trend of BLH when away from the coast was also illustrated in former satellite-based studies (Ratnam and Basha, 2010; Guo et al, 2011; Ao et al, 2012Randall et al., 1998; Palm et al., 2005; Jordan et al., 2010; McGrath-Spangler and Denning, 2012, 2013). However, due to different methodologies associated with different definition of BLH and the filtering of cloud conditions, this study shows a significant magnitude of differences in BLH form former studies. As an example, the BLH reported in McGrath-Spangler and Denning (2013) is much lower than the BLH seen in our results, but there is similarity in pattern and value of our MLH and the McGrath-Spangler and Denning BLH over the eastern Pacific Ocean.

The 4-year mean MBL coupling status in terms of averaged ratio of MLH/BLH is shown in Fig. 3 (c). The better mixed the MBL, the larger the ratio of MLH/BLH. This is shown in the stratiform cloud dominated region (where Sc Fraction > ~0.4 with stronger EIS and lower BLH) where there is higher MLH/BLH than in the cumulus cloud dominated region (where Sc Fraction<~0.4 with weaker EIS and higher BLH). The MBL is obviously decoupled over the ITCZ. The MBL shows better mixing from 100°W to 80°W of the equator, but weak mixing from 160°W to 100°W of the equator. And the decoupling trend of the MBL is present westward along the equator.

Sc occurs more frequently (Sc fraction > ~0.6) when EIS >~ 1K, with a decreasing fraction towards the far ocean, as shown in Fig. 3 (d). Sc occurrence depends on the EIS (Fig. 3 (g)), with a correlation coefficient of 0.78 at confidence level of 0.01 in their spatial patterns. Figures 3 (e) and (f) show Sc tops with and without drizzle. The Sc case is defined as the case where there are only Sc (and clear-sky if it has) profiles in the collocated 0.25° grid-box (the Sc fraction > 0). These cases are then broken into the Sc case with and without drizzle. The Sc case with drizzle is the Sc case where at least one Sc profile in the collocated 0.25° grid-box has drizzle, while the remaining Sc cases are non-drizzled Sc case. The drizzled Sc tops are lower than ~1.5 km when near the coast where the stratus cloud is dominant, and the drizzled Sc tops rise up to ~2.5 km as distance away from the coast increases. The non-drizzled Sc tops show a similar pattern to the drizzled Sc top (with a correlation coefficient of 0.53 at confidence level of 0.01 in their spatial pattern), except that the non-drizzled Sc top are lower when approaching the tropical Pacific near longitude of ~180°W. Generally, the drizzled Sc top is ~0.2 to 1 km higher than the non-drizzle Sc top, which suggests the important role of the mesoscale circulations in MBL. Precipitation more commonly occurs in updraft regions and the breakup of Sc usually happens in downdrafts areas, which was also observed in the rift area of Sc (Sharon et al., 2006) and in MAGIC (Zhou et al., 2015). Furthermore, the occurrence of drizzled Sc case is ~6.2% (the number of Sc profiles with drizzle / the number of Sc profiles) among MBL cases where a 0.25° grid-box contains both Sc and clear-sky, comparing to ~32% of all MBL cases being stratiform cloud with drizzle cases. The Sc case containing clear-sky profiles are where broken Sc clouds or a cloud edge enter a 0.25° grid-box. This relationship indicates that heterogeneous cloudy conditions within a grid-box (i.e., broken Sc clouds or near the cloud edge) are less likely to produce precipitation than where the conditions are more homogeneously cloudy.

The detailed assessments of the seasonal MBL and MBLC structures in the two selected transects over the northeastern and southeastern Pacific Ocean (NPO and SPO) are presented in Figs. 4 and 5. Figs. 4 and 5 (a1-a4) show the seasonal mean MBL structure in terms of MBL aerosol loading, overlain with seasonal mean BLH and MLH. The mean BLH, MLH and their standard deviations, show that the MBL tends to be more frequently well mixed near the coast region and be more frequently decoupled over the far ocean. This corresponds to a stronger EIS near the coast and weaker EIS over the far ocean (the black diamond-solid lines in Figs. 4 and 5 (b1-b4)). The EIS over the NPO shows negative correlation with the U_{10m}, with a correlation coefficient of -0.64 at confidence level of 0.01, but there is a positive correlation with the U_{10m} when EIS < 3 K over the SPO, with the correlation coefficient of 0.6 at confidence level of 0.01. The seasonal variations in the MBL structure are small over both the NPO and SPO regions, except that the MBL tends to be lower and better mixed near the coast region during March, April and May (MAM) and June, July and August (JJA) over the NPO, and in JJA and September, October and November (SON) over the SPO. This is likely associated with the stronger EIS (> 5 K) in these seasons than EIS (< 5 K) in the other seasons.

Surface wind speed is the main factor controlling the loading of sea salt aerosols near the surface, while its vertical distribution is closely related to the boundary layer processes (Luo et al., 2014b). When distant away from the coast, the aerosol loading (Figs. 4 and 5 (a1-a4)) in the well-mixed layer shows strong positive correlation with the U_{10m} in NPO with a correlation coefficient of 0.64 at the confidence level of 0.01. However, there is almost no correlation between them in the SPO (correlation coefficient of -0.08 at the confidence level of 0.39). In the SPO, when further east than longitude of ~-100°, the aerosol loading in the lower well-mixed layer increases with decreasing of the U_{10m}. This is attributed to lowering MLH limiting the vertical transportation. When near the coast region, the aerosol loading in the well-mixed layer has weak correlation with the U_{10m} over both regions, possibly due to the aerosol transported from the continent.

Figures 4 and 5 (c1-c4) show the mean Sc occurrences over the two regions. Over the NPO region (Fig. 4 (c1-c4)), the Sc occurrence is small near the coast and increases to a maximum of ~0.6 near the longitude of ~-130° to -135°. It then decreases when west southward towards the tropic. Over the NPO, the Sc occurrence increases with decreasing of EIS when distant from the coast to the maximum occurrence point (at longitude of ~-135°), with the correlation coefficient of -0.51 at the confidence level of 0.01. And there shows a positive correlation with EIS from the maximum occurrence point down to the equator, with the correlation coefficient of 0.92 at the confidence level of 0.01. Over the SPO region (Fig. 5 (c1-c4)), the maximum Sc occurrence point is close to the coast. Therefore, the Sc occurrence and the EIS both decrease when far away from the coast and correlate well with each other when further west than longitude of ~80°, with the correlation coefficient of 0.91 at the confidence level of 0.01. In the near-coast region, other processes such as sea-land breeze and cold current producing cold SST could affect the relationship between EIS and Sc occurrence. The drizzle occurrence showed a weak correlation with EIS in both regions (not shown here).

Figures 4 and 5 (d1-d4) show the seasonal mean $CTH_{drizzle}$ (blue diamond line) and $CTH_{no\ drizzle}$ (green diamond line) along with the seasonal mean BLH and MLH over the NPO and SPO. The $CTH_{no\ drizzle}$ is lower than the $CTH_{drizzle}$, but is close to the BLH. Over the NPO region, the $CTH_{drizzle}$ shows strong negative correlation with the EIS, with the correlation coefficients of < -0.82 at the confidence level of 0.01. Over the NPO region, in MAM, JJA and SON, the $CTH_{drizzle}$ shows strong negative correlation with the EIS, with the correlation coefficients of < -0.77 at the confidence level of 0.01, while very weak correlation in December, January and February (DJF), with the correlation coefficients < -0.33 at the confidence level of 0.08. The $CTH_{no\ drizzle}$ generally shows a weak correlation with the EIS, although there is a positive correlation with the EIS for sub-regions, such as over the SPO when west of longitude of ~-90° in DJF and MAM and when west of longitude of ~-100° in JJA and SON, with the correlation coefficients of > 0.64 at the confidence level of 0.01. The difference between $CTH_{drizzle}$ and $CTH_{no\ drizzle}$ shows strong dependence on the EIS, i.e., there is a smaller difference associated with stronger EIS and larger difference associated with weaker EIS. This is attributed to a stronger EIS indicating a more stable MABL, which allows for small depth variations associated with several possible vertical displacement forces in MBL. Thus, a small difference between $CTH_{drizzle}$ and $CTH_{no\ drizzle}$ is expected under stronger EIS.

The MBL activities are strongly connected with the large-scale stabilities. Figure 6 shows the relationships between EIS and MBL coupling structure. In Fig. 6 (a), MAGIC observations and CALIOP observations over the extended MAGIC region were sorted and averaged into different bins of EIS. Both observations from MAGIC radiosonde and CALIOP show that the MBL tends to be better mixed as EIS increases. One of the main parameters controlling the entrainment process is the inversion strength near the mixing layer top (Venzenten et al., 1999). According to the definition of EIS, it implies that a stronger EIS leads to a stronger the inversion near the mixing layer top, and a weaker the entrainment of the dry warm air above the inversion. Therefore, the relationship between EIS and MBL structure indicates that the entrainment of the dry warm air above the inversion would be the main factor controlling the MBL decoupling. It could also be expected that the SST, wind shear and surface heat flux may also affect MBL decoupling as these parameters or processes can also affect the entrainment process (Venzenten et al., 1999). However, analyses of U_{10m} and SST show only very weak correlations with MBL coupling structure. This is possibly due to the uncertainties in satellite retrievals of these parameters or that the role of other factors was partially included in the EIS.

After further investigation, we concluded that the MBL coupling structure is controlled by both LTS and EIS when EIS < ~3 K, i.e., there is greater mixing in the MBL with increasing EIS and decreasing of LTS. Fig. 6(b) shows the mean CALIOP-derived MBL coupling structure over global oceans under binned EIS and LTS values. As shown in Fig. 6(b), the mean MBL coupling structure in terms of MLH/BLH shows good correlation with EIS under different bins of LTS when LTS is between 2.5K and 17.5K (correlation coefficient of > 0.88 at confidence level of 0.01). And the MBL coupling structure in term of MLH/BLH shows a very strong negative correlation with LTS when binned EIS < 2K (correlation coefficient <-0.95 at confidence level of 0.01).

The differences between drizzling and non-drizzling Sc tops are also controlled by the EIS. Figure 6(c) shows the seasonal mean relationship over the global oceans between EIS and $CTH_{no\ drizzle}/CTH_{drizzle}$ binned by SST. The SST, EIS and $CTH_{no\ drizzle}/CTH_{drizzle}$ was averaged across a 2.5 ° x2.5° grid box and different seasons. After this, the seasonal-mean $CTH_{no\ drizzle}/CTH_{drizzle}$ was sorted and averaged into different bins of EIS and SST. This binning showed that wth cold SST (SST< =20°C) in the middle to high latitude regions, mean $CTH_{no\ drizzle}/CTH_{drizzle}$ does not vary with EIS, whereas in the Sc-to-Cu transition regions where there is warm SST (SST> 20°C), the mean $CTH_{no\ drizzle}/CTH_{drizzle}$ shows good dependence on EIS (a correlation coefficient >0.89 at confidence level of 0.01). The relative difference between $CTH_{drizzle}$ and $CTH_{no\ drizzle}$ becomes larger with decreasing EIS and increasing SST, indicating more vigorous the subsidence and uplifting in the MBL under weak EIS conditions and warmer SST. This result suggests that the subsidence and uplifting may relate to meso-scale processes, such as gravity waves, which can be generated from the geostrophic adjustment, jet break or other sources, affecting the morphology of clouds (Jiang and Wang, 2012; Allen et al., 2013) over the Sc-to-Cu transition regions. The different roles of SST and EIS in controlling Sc top and precipitation generation in different regions will be further investigated of in future studies.

10.2 Discussion

The MBL decoupling was suggested to play an important role in Sc-to-Cu transition (Bretherton and Wyant, 1997; Wood and Bretherton, 2004). The MBL structure is shown in Fig. 7 as the mean of aerosol backscattering from the cases with both clear-sky and stratiform/Cu cloud in the same 0.25° grid box over the eastern Pacific Ocean where the Sc-to-Cu transition frequently happens. The clear condition is defined as totally cloud-free in the 25 km AMSR-E footprint (named as clear MBL). This condition is expected to be less affected by the local circulation associated with the cloud development. Aerosols under the stratiform cloud condition are derived from cases with partially stratiform cloud and partially clear sky in a 0.25° AMSR-E footprint (named as stratiform MBL). Aerosols under the Cu cloud condition are derived from cases with partially Cu cloud and partially clear sky in a 0.25° AMSR-E footprint (named as Cu MBL). According to the comparison of CALIOP-derived clear-sky MBL structure with near-by cloudy-sky MBL structure from MAGIC radiosonde and with the nearby stratiform cloud top from 2B-CLDCLASS-LIDAR in section 3.2, it is reasonable to assume that the cloud-topped MBL can have the similar structure to the nearby clear-sky MBL within a 0.25° footprint for the Sc and Cu MBL cases. Figure 7 shows that the clear MBL and Cu MBL become more decoupled with increasing BLH and decreasing EIS as indicated by large vertical gradients between mixing layer aerosols and near

MBL top aerosols. The Stratiform MBL shares similar characteristics to the Cu MBL, but are better mixed than clear MBL and Cu MBL when EIS > 0. According to Fig. 3, the region with EIS < 0 K is the Cu cloud dominated region (where the fraction of Sc cloud is smaller than 0.2), and the Sc MBL cases here are more likely to associated with the clear-sky MBL adjacent to the small Sc. The region of 0 K< EIS < 2.5 K is considered a transition region where the Sc clouds are broken down and transit to Cu clouds. The Stratiform MBL cases with 0 K< EIS <2.5 K are more likely associated to the clear-sky MBL adjacent to broken Sc. The stratiform MBL cases with EIS> 2.5 K are more likely associated with the clear-sky MBL near the edge of overcast Sc in the region where Sc fraction >~0.6. When EIS < 0K, the stratiform MBL showed no major difference between clear MBL and Cu MBL. With increasing EIS, corresponding to increasing amount of stratiform clouds, the presence of large-scale subsidence prompts a well-mixed MBL, or more occasionally a decoupled MBL with two well-mixed sub-layers (Fig. 7(c2)).

11 Conclusions

This paper used 4-year satellite observations to investigate the MBL decoupled structure and its spatial distribution over the eastern Pacific region and its dependence on environmental parameters over global oceans (within latitude of ±50°). The aerosol information in CALIOP-measured backscattering data is considered to be a good proxy for the MBL decoupled structure. The aerosol layer top is a good indicator for BLH and was able be identified by the threshold method, whereas the MLH could be identified by the gradient methods. The lidar determined BLH showed good agreements with BLH determined by the RI method using radiosonde measurements and with the stratiform cloud top from CloudSat product. The lidar determined MLH showed good agreement with the base of lowest inversion layer in radiosonde temperature profiles.

The lidar methodology was then applied to the 4-year satellite observations over the eastern Pacific Ocean. Clear-sky MBL structure characteristics were analyzed together with the cloudy MBL top (inferred from the stratiform cloud top). For the first time, the climatology and seasonal variations of the MBL structure in the eastern Pacific Ocean region were presented and analyzed. This analysis showed that MBL is generally decoupled, with MLH/BLH ratio ranging from ~0.5 to ~0.8. The MBL decoupling magnitude is mainly controlled by EIS that affects the cloud top entrainment process, with correlation coefficient of > 0.88 at confidence level of 0.01 between the mean MBL coupling structure in terms of

MLH/BLH and EIS when binned LTS is between 2.5K and 17.5K. The systematic differences between drizzling and non-drizzling Sc tops over the Sc-to-Cu transition region also show dependence on EIS and may relate to the meso-scale circulations driven by gravity wave in MBL. Further analysis showed that the MBL shows similar decoupled structure under clear sky and cumulus cloud-topped conditions, but is better mixed under Sc breakup and overcast conditions.

This study demonstrated that satellite lidar measurements offer a unique opportunity to characterize MBL over global oceans, something no possible using other techniques. Multi-satellite measurements also offer a chance to further study related MBL processes. Using observational results presented here, it will be possible to evaluate and improve model MBL simulations under different dynamical and thermodynamical conditions.

Acknowledgements

This research was partially funded by the DOE Grant DE-SC0006974 as part of the ASR program and by the NASA Grant NNX13AQ41G. We would also like to thank anonymous reviewers for their positive and constructive comments. The authors would like to thank CloudSat team for providing data from the CloudSat Data Processing Center (http://www.cloudsat.cira.colostate.edu). The authors would like to thank the CALIOP team for providing data obtained from the NASA Langley Research Center Atmospheric Science Data Center. AMSR data are produced by Remote Sensing Systems and were sponsored by the NASA AMSR-E Science Team and the NASA Earth Science MEaSUREs Program and are available at www.remss.com. AIRS data were obtained through the Goddard Earth Sciences Data and Information Services Center (http://daac.gsfc.nasa.gov). The buoy data was obtained from National Data Buoy Center (http://www.ndbc.noaa.gov/). ARM data is made available through the U.S. Department of Energy as part of the Atmospheric Radiation Measurement (ARM) Program. ARM Climate Research Facility TWP-C2 site data and MAGIC campaign data were used.

References

Ahlgrimm, M. and Randall, D. A.: Diagnosing monthly mean boundary layer properties from reanalysis data using a bulk boundary layer model, J. Atmos. Sci., 63, 998-1012, 2006.

Ao, C. O., Waliser D. E., Chan, S. K., Li, J.-L., Tian, B., Xie, F., and Mannucci, A. J.: Planetary boundary layer heights from GPS radio occultation refractivity and humidity profiles, J. Geophys. Res., 117, D16117, 2012.

Albrecht, B. A., Jensen, M. P., and Syrett, W. J.: Marine boundary layer structure and fractional cloudiness, J. Geophys. Res., 100(D7), 14209-14222, 1995.

Allen, G., Vaughan, G., Toniazzo, T., Coe, H., Connolly, P., Yuter, S. E., Burleyson, C. D., Minnis, P., and Ayers, J. K.: Gravity‐wave‐induced perturbations in marine stratocumulus, Quarterly Journal of the Royal Meteorological Society, 139 (670), 32-45, 2013.

Bony, S. and Dufresne, J.-L.: Marine boundary layer clouds at the heart of tropical cloud feedback uncertainties in climate models, Geophys. Res. Lett., 32, L20806, 2005.

Boers, R., Eloranta, E. W., and Coulter, R. L.: Lidar observations of mixed layer dynamics: tests of parameterized entrainment models of mixed layer growth rate, J. Clim. Appl. Meteorol., 23, 247-266, 1984.

Boers, R. and Eloranta, E. W.: Lidar measurements of the atmospheric entrainment zone and potential temperature jump across the top of the mixed layer, Bound.-Lay. Meteorol., 34, 357-375, 1986.

Bretherton, C. S. and Wyant, M. C.: Moisture transport, lower-tropospheric stability, and decoupling of cloud-topped boundary layers, J. Atmos. Sci., 54, 148-167, 1997.

Emeis, S., Schafer, K., and Munkel, C.: Surface-based Remote Sensing of the Mixing-layer Height – a Review, Meteorologische Zeitschrift, 17, 621-630, 2008.

Guo, P., Kuo, Y.-H., Sokolovskiy, S. V., and Lenschow, D. H.: Estimating Atmospheric Boundary Layer Depth using COSMIC Radio Occultation Data, J. Atmos. Sci., 68(8), 1703–1713, 2011.

Jason, L.: README document for AIRS Level-2 version 005 standard products. Goddard Earth Sciences Data And Information Services Center (Ed., National Aeronautics and Space Administration (NASA), 2008.

Jiang, Q. and Wang, S.: Impact of gravity waves on marine stratocumulus variability, J. Atmos. Sci., 69(12), 3633-3651, 2012.

Jones, C. R., Bretherton, C. S., and Leon, D.: Coupled vs. decoupled boundary layers in VOCALS-REx, Atmos. Chem. Phys., 11, 7143-7153, 2011.

Jordan, N. S., Hoff, R. M., and Bacmeister, J. T.: Validation of Goddard Earth Observing System-version 5 MERRA planetary boundary layer heights using CALIPSO, J. Geophys. Res., 115(D24), D24218, 2010.

Kawanishi, T., Sezai, T., Ito, Y., Imaoka, K., Takeshima, T., Ishido, Y., Shibata, A., Miura, M., Inahata, H., and Spencer, R. W.: The Advanced Microwave Scanning Radiometer for the Earth Observing System (AMSR-E), NASDA's contribution to the EOS for global energy and water cycle studies, IEEE Trans. Geosci. Remote Sensing, 41, 184-194, 2003.

Klein, S. A. and Hartmann, D. L.: The seasonal cycle of low stratiform clouds, J. Climate, 6, 1587-1606, 1993

Kong, W., and Fan Y.: Convective boundary layer evolution from lidar backscatter and its relationship with surface aerosol concentration at a location of a central China megacity, Journal of Geophysical Research: Atmospheres, 120 (15), 7928-7940, 2015.

Lambrigtsen, B. H. and Lee, S.-Y.: Coalignment and synchronization of the AIRS instrument suite, IEEE T. Geosci. Remote, 41, 343-351, 2003.

Leon, D. C., Wang, Z. and Liu, D.: Climatology of drizzle in marine boundary layer clouds based on 1 year of data from CloudSat and Cloud-Aerosol Lidar and Infrared Pathfinder Satellite Observations (CALIPSO), J. Geophys. Res., 113, D00A14, 2008.

Leventidou, E., Zanis, P., Balis, D., Giannakaki, E., Pytharoulis, I., and Amiridis, V.: Factors affecting the comparisons of planetary boundary layer height retrievals from CALIPSO, ECMWF and radiosondes over Thessaloniki, Greece, Atmospheric Environment, 74, 360-366, 2013.

Lewis, E. R., and Coauthors, 2012: MAGIC: Marine ARM GPCI Investigation of Clouds. DOE/SC-ARM-12-020, U.S. Department of Energy, 12 pp.

Luo, T., Yuan, R. M. and Wang, Z.: Lidar-based remote sensing of atmospheric boundary layer height over land and ocean, Atmos. Meas. Tech., 7, 1-10, 2014a.

Luo, T., Yuan, R. M., and Wang, Z.: On factors controlling marine boundary layer aerosol optical depth, Journal of Geophysical Research: Atmospheres, 119(6), 3321-3334, 2014b.

Luo, T., Yuan, R. M., Wang, Z. and Zhang, Z.: Quantifying the Hygroscopic Growth of Marine Boundary Layer Aerosols by Satellite-Based and Buoy Observations. *J. Atmos. Sci.*, **72**, 1063-1074, 2015.

McGrath-Spangler, E. L., and Denning A. S.: Estimates of North American summertime planetary boundary layer depths derived from space-borne lidar, J. Geophys. Res., 117(D15101), 2012.

McGrath-Spangler, E. L., and Denning A. S.: Global seasonal variations of midday planetary boundary layer depth from CALIPSO space-borne LIDAR, J. Geophys. Res. Atmos., 118, 1226–1233, 2013.

Melfi, S. H., Sphinhirne, J. D., Chou, S. H., and Palm, S. P.: Lidar observations of the vertically organized convection in the planetary boundary layer over the ocean, J. Climate Appl. Me- teorol., 24, 806-821, 1985.

Minnis, P., Heck, P. W., Young, D. F., Fairall, C. W., and Snider, J. B.: Stratocumulus cloud properties derived from simultaneous satellite and island-based instrumentation during FIRE, J. Appl. Meteorol., 31, 317-339, 1992.

Norris, J. R., Leovy, C. B.: Interannual variability in stratiform cloudiness and sea surface temperature, J. Climate, 7, 1915-1925, 1994.

Norris, J. R.: Low cloud type over the ocean from surface observations. Part I: relationship to surface meteorology and the vertical distribution of temperature and moisture, J. Climate, 11, 369-382, 1998.

Overoye, K., Aumann, H. H., Weiler, M. H., Gigioli, G. W., Shaw, W., Frost, E., and McKay, T.: Test and calibration of the AIRS instrument, SPIE Proceedings, 3759, 254-265, 1999.

Pagano, T. S., Aumann, H. H., Hagan, D. E. and Overoye, K.: Prelaunch and in-flight radiometric calibration of the Atmospheric Infrared Sounder (AIRS), IEEE Trans. Geosci. Remote Sens., 41, 265–273, 2003.

Palm, S. P., Benedetti, A., and Spinhirne, J.: Validation of ECMWF global forecast model parameters using GLAS atmospheric channel measurements, Geophys. Res. Lett., 32(22), L22S09, 2005.

Partain P.: Cloudsat ECMWF-AUX auxiliary data process description and interface control document, 2004.

Piironen, P., and Eloranta, E. W.: Demonstration of a high spectral resolution lidar based on an iodine absorption filter, Optics letters, 19, 234-236, 1994.

Ratnam, M. V. and Basha, S. G.: A Robust Method to Determine Global Distribution of Atmospheric Boundary Layer Top from COSMIC GPS RO Measurements, Atmos. Sci. Let, 11, 216–222, 2010.

Randall, D. A., Abeles, J. A. and Corsetti, T. G.: Seasonal simulations of the planetary boundary layer and boundary-layer stratocumulus clouds with a general circulation model. J. Atmos. Sci., 42, 641-675, 1985.

Randall, D. A., Shao, Q., and Branson M. : Representation of clear and cloudy boundary layers in climate models, in Clear and Cloudy Boundary Layers, edited by A. A. M. Holtslag, and P. G. Duynkerke, pp. 305–322, Royal Netherlands Academy of Arts and Sciences, Amsterdam, 1998.

Randall, D.A., Wood, R.A., Bony, S., Colman, R., Fichefet, T., Fyfe, J., Kattsov, V., Pitman, A., Shukla, J., Srinivasan, J., Stouffer, R. J., Sumi, A. and Taylor, K.E.: Climate Models and Their Evaluation. In: Climate Change 2007: The Physical Science Basis. Contribution of Working Group I to the Fourth Assessment Report of the Intergovernmental Panel on Climate Change [Solomon, S., D. Qin, M. Manning, Z. Chen, M. Marquis, K.B. Averyt, M.Tignor and H.L. Miller (eds.)]. Cambridge University Press, Cambridge, United Kingdom and New York, NY, USA, 2007.

Sassen, K. and Z. Wang, 2012: The Clouds of the Middle Troposphere: Composition, Radiative Impact, and Global Distribution, Surv. Geophys., 3, 677-691, 2012.

Seidel, D. J., Ao, C. O., and Li K.: Estimating climatological planetary boundary layer heights from radiosonde observations: comparison of methods and uncertainty analysis, J. Geophys. Res., 115, D16113, 2010.

Shipley, S. T., Tracy D. H., Eloranta, E. W., Trauger, J. T., Sroga, J. T., Roesler, F. L. and Weinman, J. A.: A High Spectral Resolution Lidar to measure optical scattering properties of atmospheric aersols, Part I: Instrumentation and theory, Applied Optics, 23, 3716-3724, 1983.

Stephens, G. L., Vane, D. G., Boain, R. J., Mace, G. G., Sassen, K., Wang, Z., Illingworth, A., J., O'Connor, E. J., Rossow, W. B., Durden, S. L., Miller, S. D., Austin, R. T., Benedetti, A., Mitrescu, C., and The CloudSat Science Team: THE CLOUDSAT MISSION AND THE A-TRAIN. *Bull. Amer. Meteor. Soc.*, 83, 1771-1790, 2002.

Stull, R. B. and Eloranta, E. W.: Boundary Layer Experiment 1983, Bull. Amer. Meteorol. Soc., 65, 450–456, 1984.

Susskind, J., Barnet, C., Blaisdell, J., Iredell, L., Keita, F., Kouvaris, L., Molnar, G., and Chahine, M.: Accuracy of geophysical parameters derived from Atmospheric Infrared Sounder/Advanced Microwave Sounding Unit as a function of fractional cloud cover, J. Geophys. Res., 111, D09S17, 2006.

Tanelli, S., Durden, S. L., Im, E., Pak, K. S., Reinke, D. G., Partain, P., Haynes, J. M., and Marchand, R. T.: CloudSat's cloud profiling radar after two years in orbit: Performance, calibration, and processing. Geoscience and Remote Sensing, IEEE Transactions on, 46(11), 3560-3573, 2008.

Vanzanten, M. C., Duynkerke, P. G., and Cuijpers, J. W.: Entrainment parameterization in convective boundary layers, J. atmos. sci., *56*(6), 813-828, 1999.

Vogelzang, D., and Holtslag, A.: Evaluation and model impacts of alternative boundary-layer height formulations. Bound.-Layer Meteor., 81, 245-269, 1996.

Wang, Z., D. Vane, G. Stephens, and D. Reinke, 2012: Level 2 combined radar and lidar cloud scenario classification product process description and interface control document. JPL Rep., 22 pp. Available online at http://www.cloudsat.cira.colostate.edu/sites/default/files/products/files/2B-CLDCLASS-LIDAR_PDICD.P_R04.20120522.pdf [Accessed 2016/02/25].

Wentz, F. J., Gentemann C. and Ashcroft, P.: On-orbit calibration of AMSR-E and the retrieval of ocean products, 83rd AMS Annual Meeting, American Meteorological Society, Long Beach, CA, 2003.

Wentz, F.J., T. Meissner, C. Gentemann, and M.Brewer: Remote Sensing Systems AQUA AMSR-E Daily Environmental Suite on 0.25 deg grid, Version 7.0 . Remote Sensing Systems, Santa Rosa, CA, 2014. Available online at www.remss.com/missions/amsre [Accessed 2016/02/25].

Winker, D. M., Hunt, W. H., and McGill M. J.: Initial performance assessment of CALIOP, Geophys. Res. Lett., 34(19), L19803, 2007.

Winker, D. M., Vaughan, M. A., Omar, A., Hu, Y., Powell, K. A., Liu, Z., Hunt, W. H., and Young, S. A.: Overview of the CALIPSO mission and CALIOP data processing algorithms, J. Atmos. Oceanic Technol., (26), 2310-2323, 2009.

Wood R. and Bretherton C. S.: Boundary layer depth, entrainment, and decoupling in the cloud-capped subtropical and tropical marine boundary layer, J. Climate, 17, 3576-3588, 2004.

Wood, R., and Bretherton, C. S.: On the relationship between stratiform low cloud cover and lower-tropospheric stability, J. Climate, 19(24), 6425–32, 2006.

Wyant, M. C., Wood, R., Bretherton, C. S., Mechoso, C. R., Bacmeister, J., Balmaseda, M. A., Barrett, B., Codron, F., Earnshaw, P., Fast, J., Hannay, C., Kaiser, J. W., Kitagawa, H., Klein, S. A., Köhler, M., Manganello, J., Pan, H.-L., Sun, F., Wang, S., and Wang, Y.: The PreVOCA experiment: modeling the lower troposphere in the southeast Pacific, Atmos. Chem. Phys., 10, 4757-4774, 2010.

Wyant, M. C., Bretherton, C. S., Wood, R., Carmichael, G. R., Clarke, A., Fast, J., George, R., Gustafson Jr., W. I., Hannay, C., Lauer, A., Lin, Y., Morcrette, J.-J., Mulcahy, J., Saide, P. E., Spak, S. N., and Yang, Q.: Global and regional modeling of clouds and aerosols in the marine boundary layer during VOCALS: the VOCA intercomparison, Atmos. Chem. Phys., 15, 153-172, 2015.

Xie, F., Wu, D. L., Ao, C. O., Mannucci, A. J., and Kursinski, E. R.: Advances and Limitations of Atmospheric Boundary Layer Observations with GPS Occultation over Southeast Pacific Ocean, Atmos. Chem. Phys., 12, 903-918, 2012.

Yue, Q., Kahn, B. H., Fetzer, E. J., and Teixeira, J.: Relationship between marine boundary layer clouds and lower tropospheric stability observed by AIRS, CloudSat, and CALIOP, J. Geophys. Res.,116, D18212, 2011.

Zhou, X., Kollias, P., and Lewis, E. R.: Clouds, precipitation, and marine boundary layer structure during the magic field campaign. J. Climate, 28, 2420–2442, 2015.

Zhang, C., Wang, Y., Hamilton, K.: Improved representation of boundary layer clouds over the southeast Pacific in ARW-WRF using a modified tiedtke cumulus parameterization scheme, Mon. Wea. Rev., 139, 3489-3513, 2011.

Zhou, X., Kollias, P., and Lewis, E. R.: Clouds, precipitation and marine boundary layer structure during the MAGIC field campaign, Journal of Climate, 28, 2420-2442, 2015.

Zuidema, P., Painemal, D., Szoeke, S. de, Fairall, C.: Stratocumulus cloud-top height estimates and their climatic implications, J. Climate, 22, 4652-4666, 2009.

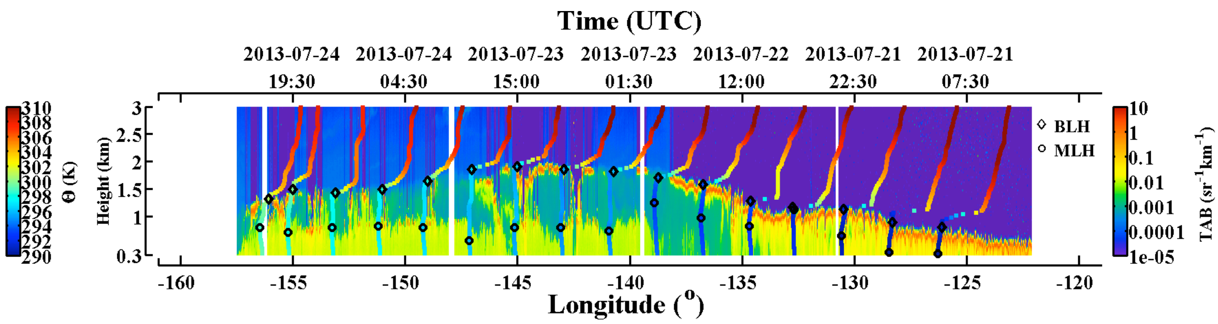

Figure 1. Potential temperature profiles and retrieved MBL structure (black diamonds for BLH and black circles for MLH) for a MAGIC leg from 2013/07/21 - 2013/07/24, overlaid with total attenuated backscattering from HSRL.

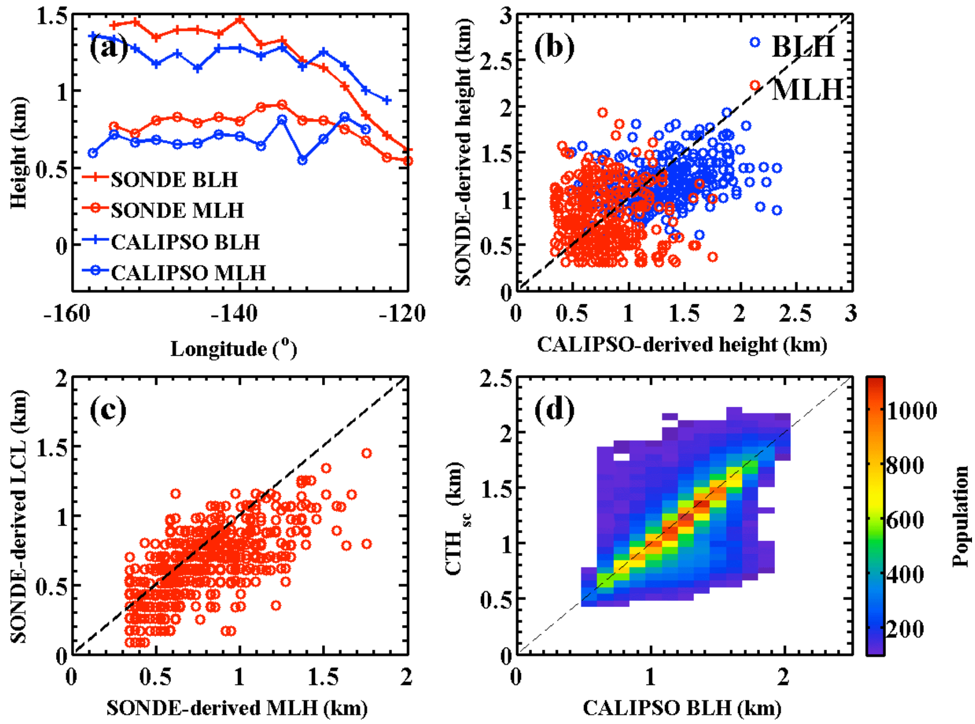

Figure 2. (a) Mean MBL structure along longitude from MAGIC radiosonde and collocated CALIOP observations; (b) comparisons of radiosonde and CALIOP derived BLH and MLH; (c) comparison of radiosonde derived MLH and LCL; (d) comparison of CALIOP derived BLH and stratiform cloud top (CTH_{sc}).

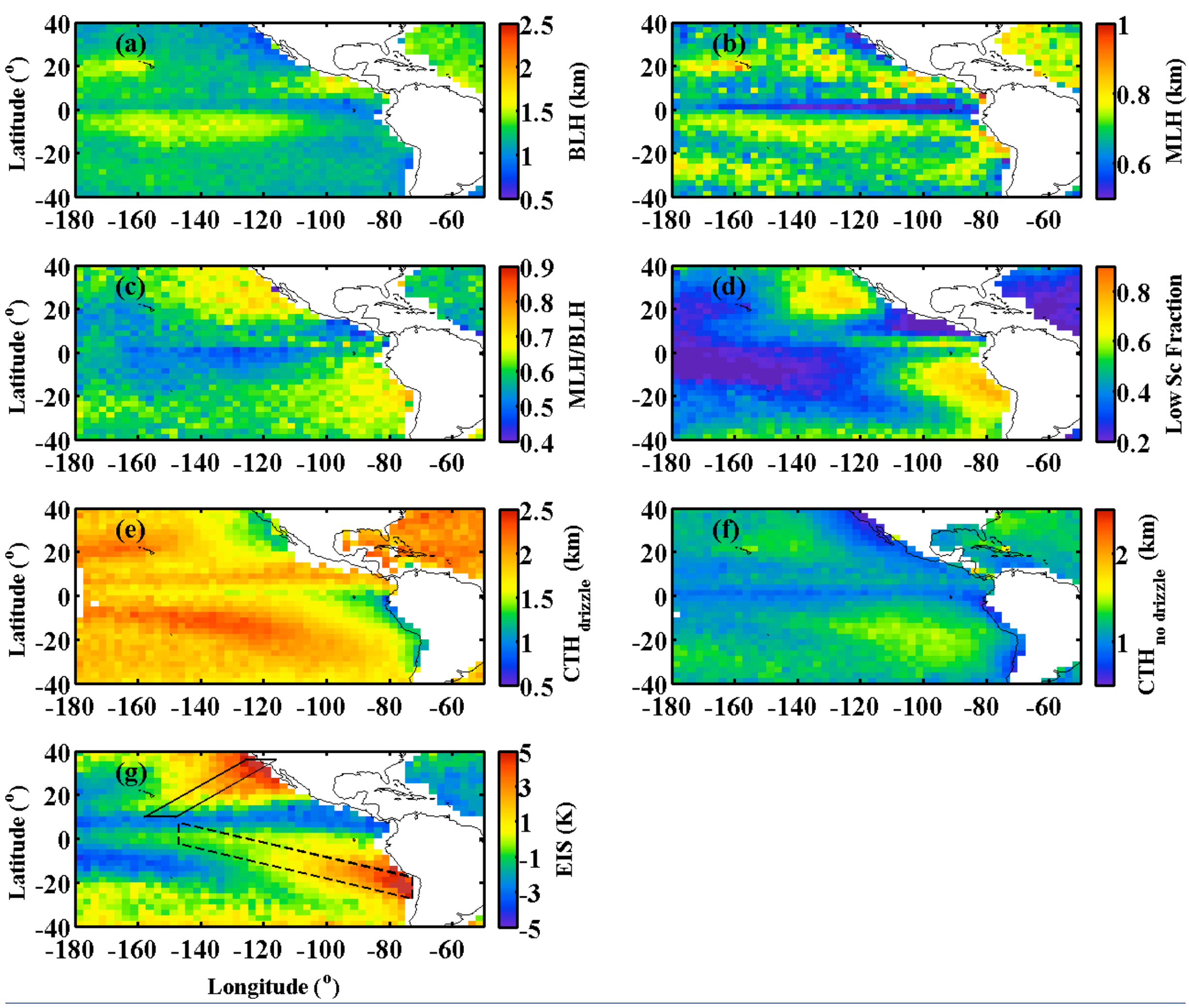

Figure 3. The spatial distribution of (a) CALIOP derived BLH, (b) CALIOP derived MLH, (c) CALIOP derived MBL decoupling structure in term of MLH/BLH, (d) Marine low clouds fraction, (e) drizzled stratiform CTH ($CTH_{drizzle}$), (f) non-drizzled stratiform CTH ($CTH_{no\ drizzle}$), (g) EIS. The solid and dashed boxes in (g) denote the selected transects on the northeastern and southeastern Pacific Ocean (NPO and SPO) used in Figs. 4 and 5 respectively.

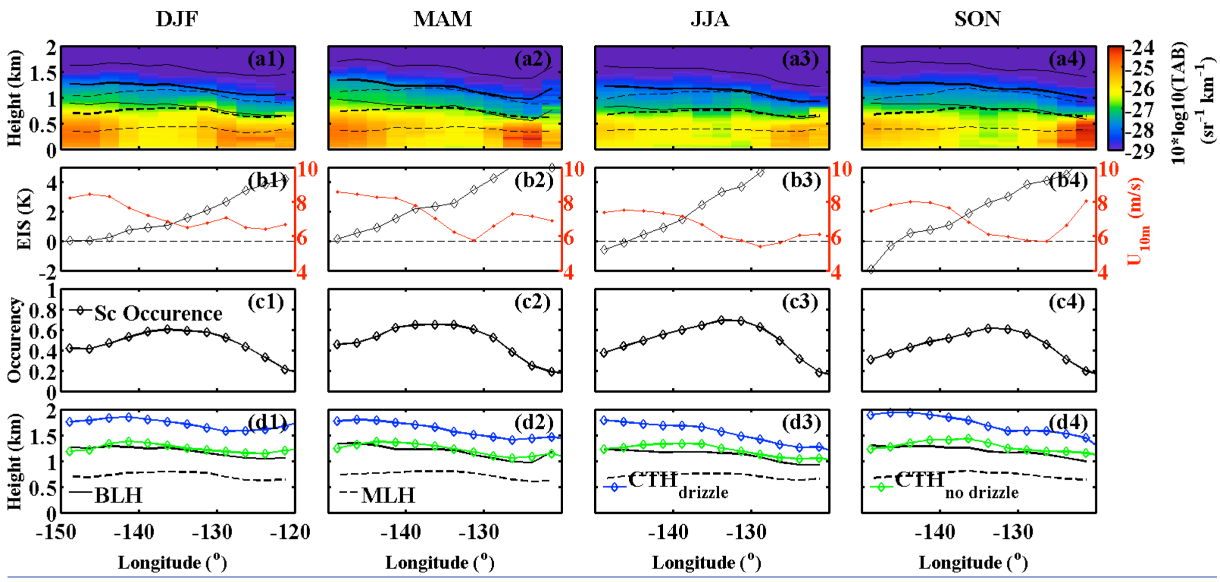

Figure 4: The satellite MBL observations along the transect region on the northeastern Pacific Ocean (NPO, solid box in fig 3e) in different seasons: (a1-a4) the mean BLH (solid line) and MLH (dashed line) overlaid with TAB, and corresponding standard deviations (thin solid and dashed lines); (b1-b4) EIS (black diamond line) and U_{10m} (red dot line); (c1-c4) stratocumulus (Sc) occurrence; (d1-d4) comparisons of BLH, MLH, $CTH_{drizzle}$, and $CTH_{no\ drizzle}$.

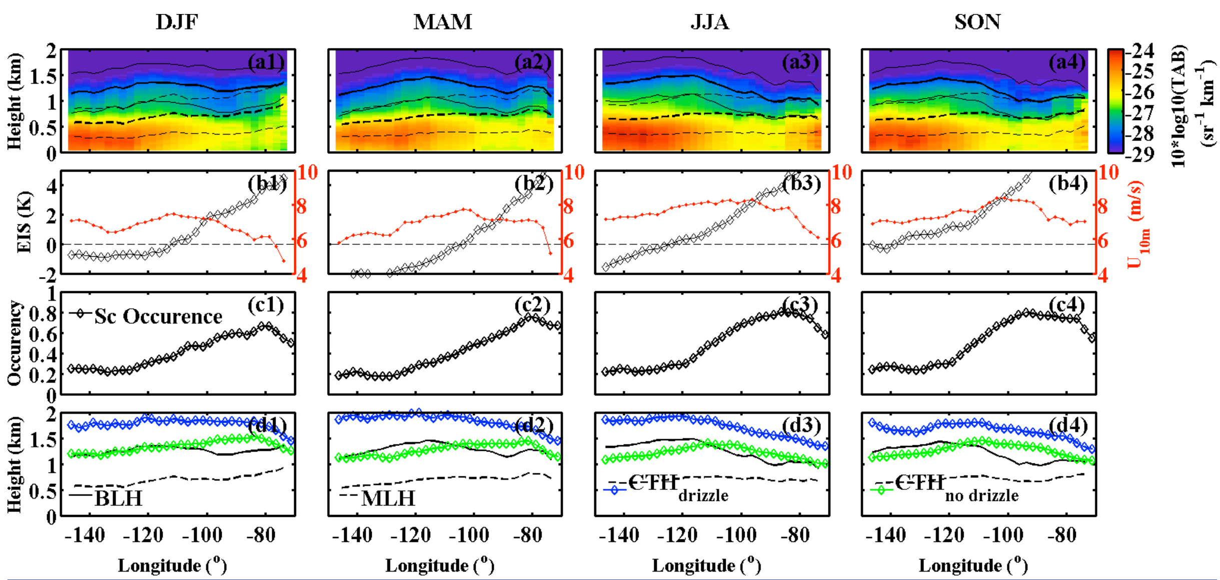

Figure 5: Same as Fig. 4 but for the transect region on the southeastern Pacific Ocean (SPO, dashed box in fig 3e) in different seasons.

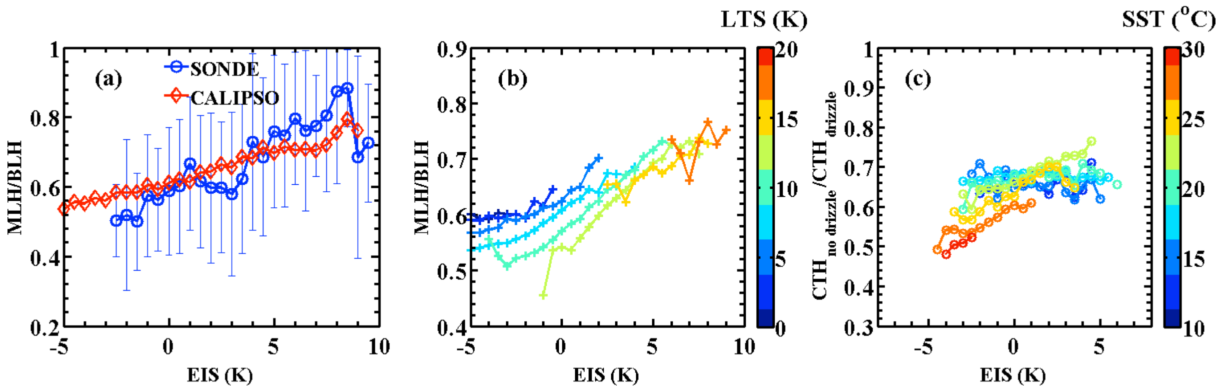

Figure 6. (a) Relationship with EIS and MLH/BLH in MAGIC and Satellite observations over extended MAGIC region; (b) relationship between EIS and CALIOP-derived MLH/BLH under different LTS over the global oceans; (c) seasonal mean relationship between EIS with $CTH_{no\ drizzle}/CTH_{drizzle}$ under different SST over the global oceans. The standard deviations in the figures (a) and (b) are ~0.2, and ~0.1 in (c).

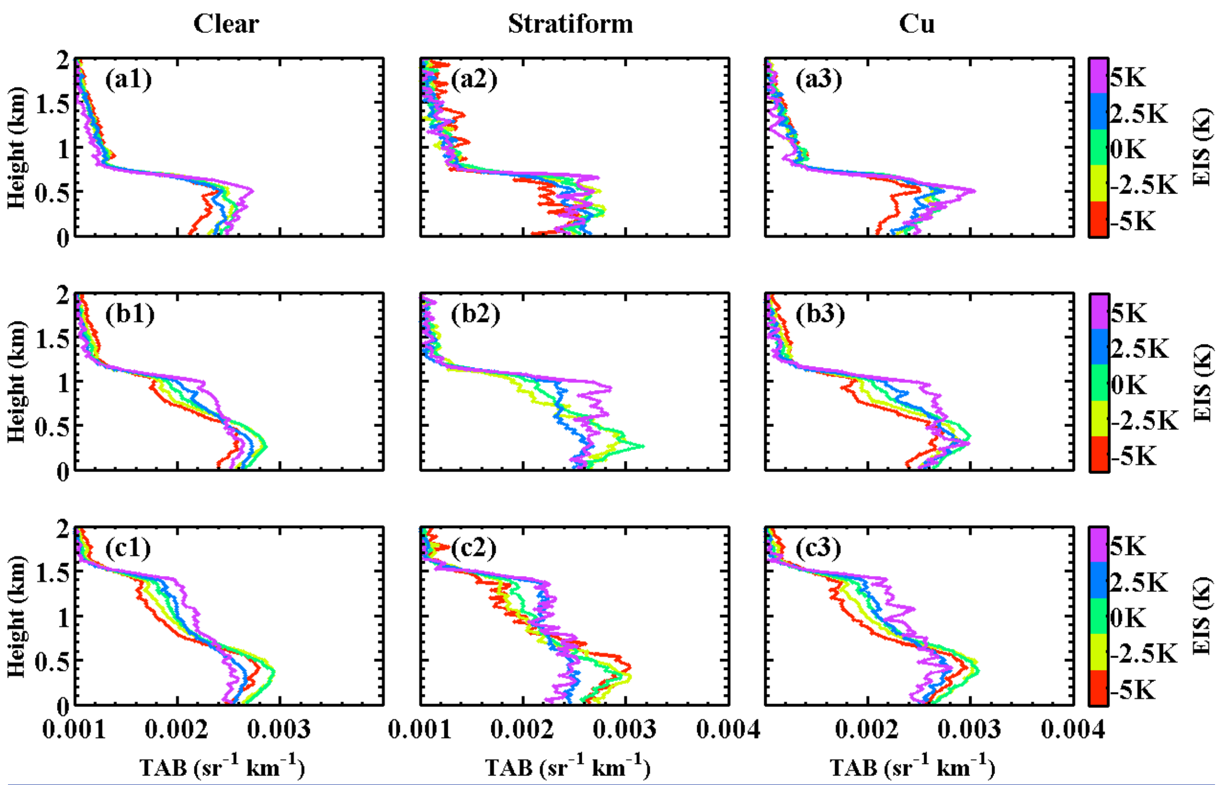

Figure 7. Mean MBL CALIOP TAB structure under different conditions from 4-year climatology over the eastern Pacific Ocean: 0.6km < BLH < 0.8 km (a1, a2, a3), 1 km < BLH < 1.2 km (b1, b2, b3), and 1.4 km < BLH < 1.6 km (c1, c2, c3). (a1, b1, c1) are under the clear conditions that is defined as totally cloud-free over a 0.25° AMSR-E footprint; (a2, b2,

c2) are under the stratiform cloud conditions that is defined as with only stratiform cloud and clear sky in each 0.25° AMSR-E footprint; (a3, b3, c3) are under the Cu cloud conditions that is defined as with only Cu cloud and clear sky in each 0.25° AMSR-E footprint. Only results with 5 m/s < U_{10m} < 8 m/s were included.